
**Addis Ababa University**
**Addis Ababa Institute of Technology**
**School of Electrical and Computer Engineering**

# Analysis and DSP Implementation of Sensorless Speed Control of Induction Motor Using Model Reference Adaptive Controller and Luenberger Observer

By: **Dita Tilahun Kassaye**

Thesis Submitted To Addis Ababa Institute of Technology in Partial Fulfillment of the Requirements for the Degree of Master of Science in Electrical and Computer Engineering (Control Engineering)

Advisor:
**Dr. Mengesha Mamo**

**June 10, 2020**
**Addis Ababa,Ethiopia**

**Addis Ababa University**
**Addis Ababa Institute of Technology**
**School of Electrical and Computer Engineering**

Analysis and DSP Implementation of Sensorless Speed Control of Induction Motor Using Model Reference Adaptive Controller and Luenberger Observer

By:
Dita Tilahun Kassaye

Approval by board of examiners

| | | |
|---|---|---|
| Dr. Yalemzewd Negash | _____ | _____ |
| Chairman, Department of Graduate Committee | Signature | Date |
| Dr. Mengesha Mamo | _____ | _____ |
| Thesis Supervisor | Signature | Date |
| Dr. Lebsework Negash | _____ | _____ |
| Internal Examiner | Signature | Date |
| Mr. Yared Tadesse | _____ | _____ |
| External Examiner | Signature | Date |

**Declaration:**

This thesis is a presentation of my original research work. Wherever contribution of others are involved, every effort is made to indicate this clearly, with proper citation of sources. I, the under signed, declare the thesis has not been presented for degree in any other university.

| | |
|---|---|
| Dita Tilahun Kassaye | _____ |
| Name | Signature |
| Addis Ababa, Ethiopia | June 10, 2020 |
| Place | Date of Submission |

This thesis has been submitted with my approval as a university advisor.

| | |
|---|---|
| Dr. Mengesha Mamo | _____ |
| Thesis Supervisor | Signature |

**Acknowledgment:**

I would like to express my most sincere acknowledgment to my Supervisor Dr. Mengesha Mamo for his support and guidance over the course of this thesis.

I would like to thank Mr. Teshome Hambissa for his kind cooperation and encouragement in the final implementation of the thesis work.

I would like to thank my friends, especially Semere G/Leul and Yared Getahun for giving me many helpful comments and emotional support.

My final gratitude goes to: my wife Roza Abebe. Had she not been by my side, the completion of this thesis wouldn't have been possible.

**Abstract:**
In this thesis, a model reference adaptive system (MRAS) and Luenberger observer (LO) based speed estimator is designed to control the speed of induction motor with no mechanical speed sensor. The proposed method involves two models, reference and adaptive model for the estimation of rotor fluxes and speed. The identified rotor fluxes from the Luenberger observer system (reference system) are used for the identification of rotor angular speed in the adaptive model. Induction motor is highly sensitive to motor parameter variation at low and zero speed. To overcome this parameter mismatch stability analysis is carried out. So that feasible range of operation is well known.

Model reference adaptive system (MRAS) and Luenberger observer (LO) based sensorless speed estimator was analyzed in terms of different reference input tracking capability, torque response quickness, low speed behavior, response of drive with speed reversal, sensitivity to motor parameter variation. The system gives good performance at low speed and both at no load and loaded condition. From the simulation results, the rotor speed is estimated with a steady state error of 0.4% and good transient response with rise time of 0.023 second and settling time of 0.05 second. Rotor flux is estimated with 0.024 second rise time, 0.2% steady state error and settling time of 0.05 second. Stator flux is estimated with 0.02 second rise time, 2% second steady state error, settling time of 0.03 second and 17% of maximum overshoot.

The proposed sensorless vector control operation is verified by simulation on MATLAB/Simulink and closed loop demonstration using Texas Instruments HVMTRPFCKIT with TMS320 F28035 DSP piccolo control card on 180w induction motor. From the demonstration work the rotor speed of the motor with maximum steady state error of 0.1800537% has been achieved under no load condition.

**Keywords:** Induction motor, Vector control, Direct field oriented control, MRAS, LO, Sensor-less, Low speed, Piccolo$^{TM}$ TMS320F28035 Control Card

# Contents

# List of Figures

# List of Tables

# List of Symbols and Abbreviations

| | | |
|---|---|---|
| $p$ | No. of poles | 8 |
| $T_e$ | Electromagnetic torque | 8 |
| $V_{sd}^{dcpl}$ | Direct axis stator voltage decoupling | 8 |
| $V_{sq}^{dcpl}$ | Quadrature axis stator voltage decoupling | 8 |
| $\gamma_0$ | Bounded positive constant | 28 |
| $\lambda$ | Positive constant | 29 |
| $\omega_r$ | Rotor speed | 8 |
| $\omega_e$ | Field speed | 8 |
| $\omega_{slp}$ | Slip speed | 8 |
| $\sigma$ | Leakage coefficient | 8 |
| $\theta_e$ | Rotor flux position | 10 |
| *AC* | Alternating current | 1 |
| *ADC* | Analog to digital converter | 46 |
| *ANN* | Artificial Neural Network | 2 |
| *B* | Viscous friction | 12 |
| *BJT* | Bipolar junction transistor | 20 |
| *BW* | Bandwidth | 12 |
| *CFI* | Current Fed Inverter | 20 |
| *CSI* | Current Source Inverter | 20 |
| $d-q$ | Direct and Quadrature | 8 |
| *DC* | Direct current | 1 |

| | |
|---|---|
| $DFOC$ | Direct field oriented control . . . . . 9 |
| $DMC$ | Digital motor control . . . . . 46 |
| $DSP$ | Digital signal processing . . . . . 1 |
| $ECAP$ | Enhanced Capture . . . . . 46 |
| $EKF$ | Extended kalman filter . . . . . 2 |
| $ELO$ | Extended Luenberger Observer . . . . . 3 |
| $EMF$ | Electromagnetic force . . . . . 22 |
| $ePWM$ | enhanced Pulse width modulator . . . . . 46 |
| $f_s$ | Switching frequency . . . . . 16 |
| $FOC$ | Field oriented control . . . . . 9 |
| $G$ | Luenberger gain . . . . . 22 |
| $GPIO$ | General input output . . . . . 46 |
| $GTO$ | Gate turn off thyristor . . . . . 20 |
| $HVMTRPFCKIT$ | High Voltage Motor Control and PFC Kit . . . . . iv |
| $I_s$ | Stator current . . . . . 13 |
| $IFOC$ | Indirect field oriented control . . . . . 9 |
| $IGBT$ | Insulated gate bipolar transistor . . . . . 20 |
| $IM$ | Induction motor . . . . . 4 |
| $J_M$ | Moment of inertia . . . . . 12 |
| $k$ | Constant obtained by pole placement . . . . . 27 |
| $k_i$ | Integral gain . . . . . 12 |
| $k_p$ | Proportional gain . . . . . 12 |
| $L_m$ | Mutual inductance . . . . . 8 |
| $L_r$ | Rotor inductance . . . . . 8 |
| $L_s$ | Stator inductance . . . . . 8 |
| $LO$ | Luenberger Observer . . . . . 2 |
| $MI$ | Modulation index . . . . . 18 |

| | |
|---|---|
| $MMF$ | Magnetomotive force ..... 15 |
| $MOSFET$ | Metal-oxide semicondactor field effect transitor ..... 20 |
| $MRAS$ | Model Reference Adaptive System ..... 2 |
| $P$ | System state vector covariance matrix ..... 22 |
| $PI$ | Proportional integral controller ..... 12 |
| $Q$ | System noise vector covariance matrix ..... 22 |
| $QEP$ | Quadrature Encoder Pulse ..... 46 |
| $R$ | Measurement noise vector covariance matrix ..... 22 |
| $R_r$ | Rotor resistance ..... 8 |
| $R_s$ | Stator resistance ..... 8 |
| $SMO$ | Sliding Mode Observer ..... 3 |
| $SVPWM$ | Space vector pulse width vector control ..... 15 |
| $T$ | Sampling time ..... 13 |
| $T_a$ | Phase A switching function ..... 17 |
| $T_b$ | Phase B switching function ..... 17 |
| $T_c$ | Phase C switching function ..... 17 |
| $THD$ | Total harmonic distortion ..... 15 |
| $V$ | Lyapunov's function ..... 29 |
| $V_{ref}$ | Reference voltage vector ..... 17 |
| $V_{s\alpha}$ | Alpha axis stator voltage ..... 17 |
| $V_{s\beta}$ | Beta axis stator voltage ..... 17 |
| $VFD$ | Variable frequency Drive ..... 9 |
| $VFI$ | Voltage Fed Inverter ..... 20 |
| $VSI$ | Voltage Source Inverter ..... 20 |
| $ZOH$ | Zero order hold ..... 13 |
| $\psi_{rd}$ | Direct axis stator flux ..... 8 |
| $\psi_{rq}$ | Quadrature axis stator flux ..... 8 |

| | | |
|---|---|---|
| $\tau_r$ | Rotor time constant | 8 |
| $\tau_s$ | Stator time constant | 8 |
| $I_{sd}$ | Direct axis stator current | 8 |
| $I_{sq}$ | Quadrature axis stator current | 8 |
| $U_{sd}$ | Direct axis stator voltage | 8 |
| $U_{sq}$ | Quadrature axis stator voltage | 8 |
| $U_{s\alpha,\beta}$ | Stationary reference frame phase voltage | 25 |
| $V_{dc}$ | DC bus voltage | 17 |

# 1 Introduction

## 1.1 Background of the Study

For many decades DC motors were widely used for variable-speed drive, for their flux and torque can be controlled in simple way, that is by varying armature current and fixing field flux. Specifically, separately excited DC motor is much easier to control. For this reason, it is used in areas where fast response and four quadrant operation with high performance at low speed is required. However, existence of commutator and brushes in DC motors raises need for intermittent maintenance. Some disadvantages occurred by the commutator and brushes are maximum cost, unable to be used in explosive or harsh environments and under high voltages and speed the commutator performance is poor. [34].

To overcome these drawbacks alternating current motors are a good choice as they are simple and rugged in structure, economical (no need of frequent maintenance), they are also robust and resistant to heavy overloading. Compared to DC motors the dimension of AC motors is smaller, this allows AC motors to be designed with noticeably better output rating, and give a better response for low weight and rotating mass [34]. Although it has all these advantages, its usage was limited. But in recent years' advancement in field of power electronics, ongoing trend toward fast switching frequency static inverters, cheaper and more effective power converters make AC motors famous in multi-motor systems. From different AC motor drives, cage induction motor has a better cost advantage. It is simple and robust and cheapest of all available motors of the same power rating. With an advancement in static converters, their outstanding speed control capabilities, variable speed drives and torque control can compete with high performance four quadrant DC motor drives. Field oriented control technique integrating fast microprocessors and digital signal processing (DSP) have made possible induction motor to replace DC motors. However the sensored speed control of induction motor still has drawbacks, that is, mechanical sensors are expensive, could be damaged and insulation is difficult. Consequently finding ways to get riding out of these sensors have been great interest in the research community for more than three decades. And developing a high performance induction motor drive independent of sensor is still a hot research area. Therefore, observers have been suggested to overcome the problems with sensors, which gives rise to the concept of sensor-less speed control. Sensor-less speed control of induction motor

is a better choice, as it has lower cost, reduced size of motor body, and absence of sensor cables. For all these advantages sensor-less speed control mechanism has got many application in areas where speed regulation and load torque immune and speed tracking is needed, although estimation of the rotor speed is dependent on the variation of the motor parameters [34].

In sensor-less speed control of induction motor terminal voltages and currents are used to estimate the speed [36]. This method includes open loop speed calculator and closed loop speed estimators where the correcting feedback is used with the motor model itself to increase the estimation accuracy. Closed loop speed estimation techniques are many in numbers, some of them are Model Reference Adaptive System (MRAS), Extended kalman filters (EKF), Luenberger Observers(LO) and Artificial Neural Network (ANN). All these closed loop methods are motor parameter dependent; therefore parameter variations can decrease speed estimation accuracy. But still these observers are good choices for fast speed estimation and, are suitable for direct use of speed feedback control.

## 1.2 Statement of the Problem

Sensor-less speed control of induction motors (IM) has been broadly studied and presented in many literatures, as expelling of speed sensor brings on the aftermath of lower cost and size, higher reliability and non frequent maintenance requirements. Observer-based analysis methods are very universal and versatile. It provides robustness as well as higher accuracy over a wide speed range with comparatively simple for realization [39].

Many machine (induction) control strategies have been developed. The Field oriented control (FOC) and Direct torque control (DTC) are industrial standard. Both are high performance, but also suffer from certain disadvantages [23, 3]. FOC uses multiple co-ordinate transformation to decouple torque and flux components of the machine. DTC uses two hysteresis comparators for torque and flux control and a predefined lookup-table containing the voltage vectors, which generate the switching pulses for the inverter. The two hysteresis comparators establish very large amount of torque ripple which worsen in the lower speed range [3].

In sensor-less speed control of induction motor, low speed and frequency performance are the main problems [22]. Speed estimation with Kalman Filters or Extended kalman filters (EKF), Luenberger observers or Extended Luenberger observers (ELO), Model eference adaptive controller (MRAC) or Artificial Neural Network (ANN) are the best estimators. However, they are computationally intensive and the choice of weighting matrices is difficult for the case of EKF and ELO, for MRAC its adaptation mechanism is simpler to design and easy to implement but it has problems of estimating accurately at low speed range [28, 36]. And for the ANN case training the neural network needs to get right data for all possible cases for a high accuracy estimation and it is application specific [33].

A lot of MRAS schemes based on rotor flux, reactive power, active power, electromagnetic torque, fictitious quantity and back emf are available in many literatures. Rotor flux based MRAS is the

simplest approach to estimate the speed of AC machine drives compared to others [3].

Luenberger observer gives good estimation result at low speed (3rpm or 0.314 rad/sec) and low frequency range [39, 33]. And as stated above, Model reference adaptive controller is simple to design and best choice for adaptation law design, for other than low speed range. So in this thesis basic Luenberger Observer and Model Reference Adaptive Controllers are associated to use the advantage of Luenberger Observer at lower speed and frequency range and advantage of model reference adaptive controller at higher speed range, for its simplicity to implement and design of its adaptation law.

## 1.3 Literature Review

A comparative study among Luenberger observer, Sliding Mode Observer and Extended Kalman filter for sensor-less vector control of induction motor drives was carried out by (Y.Zhang, Z.Zhao, T.Lu, L.Yuan, W.Xu and J.Zhu, 2009). All the three observers show high accuracy at high speed operation. Both Sliding Mode Observer (SMO) and Luenberger Observer (LO) can operate at very low speed of 15rpm with full load and 3rpm under no-load condition. SMO response showed more ripples, may be caused by the sign function. The simulation and experimental result demonstrated that LO and SMO showed strong robustness to motor parameter deviations, such as stator resistance, mutual inductance, and so on. At low speed range, robustness of Extended Kalman Filter (EKF) relative to both SMO and LO was mediocre. For EKF, initial value determination of matrix Q and R is problematic. The computational complexity of SMO and LO are nearly similar. LO and SMO provides similar overall performance at steady state and low speed operation but SMO is resistant to parameter variation. EKF is the most convoluted to implement it in DSP. However, EKF has best noise immunity. LO and SMO are Pragmatical than EKF.

Sensor-less vector control and selection of observer gain for speed control of indirect vector control induction motor drives by (S.Saha and B. Nayak, 2017) was done to compare the performance of LO and MRAS. The Model Reference Adaptive Control scheme for speed estimation posses slow dynamics compared to Luenberger adaptive control scheme. The input tracking capability is slightly affected during transient state with overshoot of 14.31%. The speed overshoots to 1310 rpm for 1146rpm step input, in model reference adaptive control method. The settling time of both methods is same(1.9second).

Model Reference Adaptive System with simple sensor-less flux observer for induction motor drive by (M. R. Khan and A. Iqbal, 2012) was studied by associating the LO with MRAS. In practical case the voltage model fails at lower speed because of dominant effect of stator resistance and DC drift. Therefore, they replaced voltage model by a simple closed loop observer(LO) with proportional gain (G). A good tracking capability even at very low speed range is achieved. The rated speed response has (Rise time 1 sec, Settling time 4 sec, and Overshoot 10%) and rated rotor flux has (Rise time 1.5 sec, Settling time 8 sec, and Overshoot 9%).

Non-proportional full-order Luenberger observers of induction motors was studied by (T.Białoń , A. Lewicki , M.Pasko and R.Niestrój, 2018). Among all types of Luenberger observers, only proportional ones are commonly applied in induction motor control systems. A typical non-proportional observer is a proportional-integral observer that provides stronger reconstruction error attenuation than a proportional observer. The greater the number of integrators, the stronger is compensation of reconstruction errors caused by the presence of unknown disturbances. However, when more integrators are applied, observer's robustness against measurement noises is less.

All of the aforementioned techniques present a good performance. But in term of fast response, good transient, steady state response, and low speed performance of the DFOC involving LO and MRAS with PI compensation used for the sensor-less speed estimation is superior. In addition robustness against parametric variations, external disturbance rejection is good.

## 1.4 General and Specific Objective of the Study

The **general objective** of this thesis is to design and show closed loop practical demonstration of Model Reference Adaptive Controller and Luenberger Observer model for speed estimation of IM which overcomes the estimation problem at low speed, load torque variation and problems of mechanical speed sensor, and with **specific objectives** of:

- Design and implementation MRAC and LO model for speed estimation
- To design PI speed and current controller for the induction motor
- Estimation of the rotor speed, rotor and stator flux

## 1.5 Methodology

Implementation of a sensor-less speed control of induction motor using Luenberger observer and model reference adaptive system speed estimator is shown in Figure 1.1. In this thesis work, Direct field oriented control method is used for sensor-less speed control of induction motor. To overcome the problem of estimators at low speed, the Luenberger Observer and Model Reference Adaptive Control models are designed with PI adaptation for the Luenberger gain part instead of only proportional gain, which makes this approach different from previous works. The added integrator makes stronger compensation of reconstruction errors caused by the presence of unknown disturbances. Reference model (LO) is used to estimate stator flux (current) and the adaptive model is used to estimate the rotor flux. The PI gains of the adaptive controller are calculated by finding the transfer function from the system block diagram. The mathematical modeling of the induction motor is derived from it's equivalent circuit diagram. Based on the mathematical modeling overall block diagram, simulation using MATLAB/Simulink is performed, and closed loop practical demonstration using Texas Instrument HVMTRPFCKIT with Piccolo TMS320 F28035 control card is carried out.

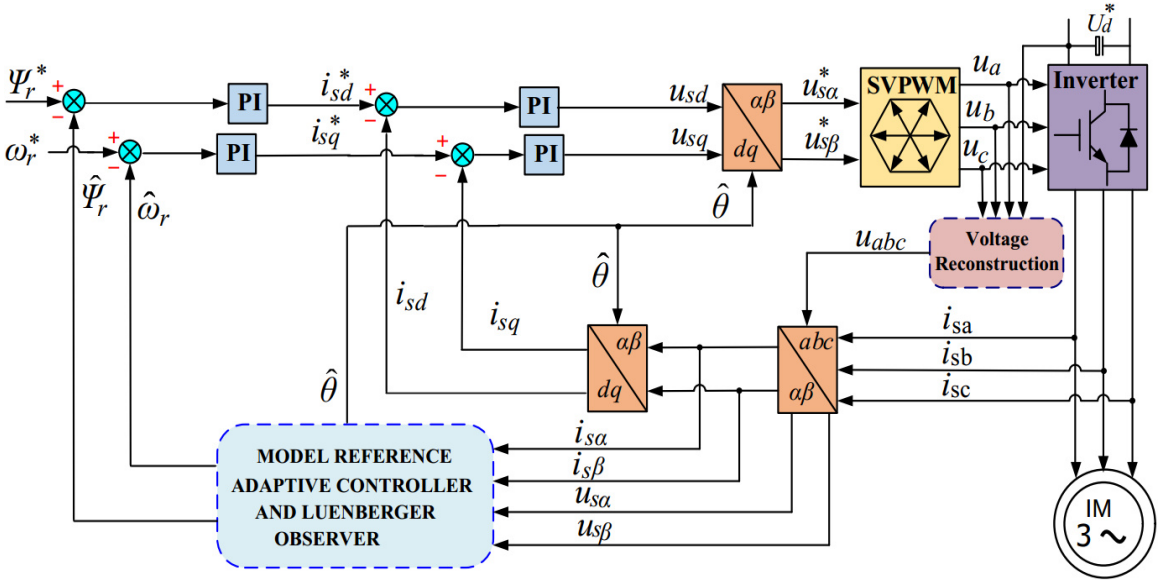


**Figure 1.1:** General block diagram of LO and MRAS based sensorless speed control of induction motor updated from [37]

## 1.6 Thesis Organization

This thesis contains six chapters, including this introduction part. The remaining chapters are organized as follows.

In the second chapter, Park and Clarke transformation, dynamic modeling and control methods are discussed. Current and flux controller are designed. At the end of this chapter, Space Vector Pulse Width Modulation implementation and two level inverters are also discussed.

In the third chapter, induction motor speed estimation methods are discussed in detail. Stator current based Luenberger Observer and rotor flux based Model Reference Adaptive System are designed. At the end of this chapter stability analysis using Lyapunov's stability and Popov's hyper-stability analysis are discussed.

In the fourth chapter, the drive system is designed in MATLAB/Simulink. It is simulated for different input values of rotor speed and flux and the simulation result is interpreted. In addition load torque variation and motor parameters variations effect is on the performance of the model is discussed.

In the fifth chapter, the closed loop experimental implementation set up, hardware and software requirements, control algorithm development are discussed. Moreover, demonstration using Texas instrument TMS320F28035 control card on general purpose AC induction motor is presented and the output is discussed.

In the last Chapter conclusion of the overall work is concluded, and recommendations for further work are given.

# 2 Induction Motor Drive

## 2.1 Introduction

For its relatively low cost, simple and rugged construction, non frequent maintenance requirements, and good operating feature, induction motor is the most commonly used type of AC motor. Induction motors range in size from a fractional horse power to about 40,000hp. Fractional-horsepower motors are usually single phase and are used widely in home, such as refrigerators, washers, dryers, and blenders. Large induction motors (usually above 5hp) are always designed for three-phase operation to achieve a constant torque and balanced network loading. In particular, where very large machinery is to be operated, the three-phase induction motor is the workhorse of the industry. In contrast to DC motors, induction motors can operate from supplies in excess of 10kV [7].

## 2.2 Dynamic Modeling of Induction Motor

The objective of the induction motor model is to give a ground to the simulation software and to understand how the model is implemented. The control system and estimation procedures are definition of a mathematical model of the machine. It is also necessary for simulation studies. In order to model the induction motor some simplifying assumption taken are, the machine is three-phase symmetrical, an air gap is constant, Iron losses are negligible, magnetic circuit is linear, without a saturation effect, motor parameters (resistance, inductance) are constant, conductor skin effect is neglected, stator windings are distributed spatially, power losses in the magnetic elements are negligible and stator winding is star connected without a neutral conductor [9].

For good understanding of dynamic modeling different reference frame transformations should be discussed first although not in detail.

### Three Phase Park Transformation

Park transformation is a well-known conversion that transforms the three phase quantities into two phase synchronously rotating reference frame for three phase inputs. The transformation has the following form [32]:

$$\left[T_{dq0}\right] = \left[T_{dq0}(\theta_d)\right]\left[f_{abc}\right] \tag{2.1}$$

Where the dq0 transformation matrix is defined as:

$$\left[T_{dq0}(\theta_d)\right] = \frac{2}{3}\begin{bmatrix} \cos\theta_d & \cos\left(\theta_d - \frac{2\pi}{3}\right) & \cos\left(\theta_d + \frac{2\pi}{3}\right) \\ -sin\theta_d & -\sin\left(\theta_d - \frac{2\pi}{3}\right) & -\sin\left(\theta_d + \frac{2\pi}{3}\right) \\ \frac{1}{2} & \frac{1}{2} & \frac{1}{2} \end{bmatrix} \tag{2.2}$$

The relation between $\theta_d$ and $\theta_q$ is given by :

$$\theta_q = \theta_d + 90^\circ \tag{2.3}$$

### Three Phase Clarke Transformation

The Clark transformation is used to transform three phase quantities to two phase quantities. The $\alpha$ -axis coincides with the phase a-axis and the $\beta$-axis leads the $\alpha$ -axis by 90°.

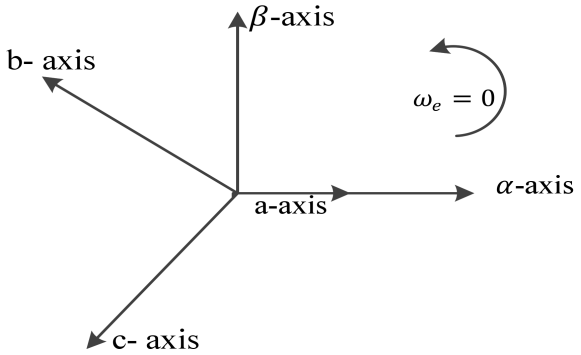


**Figure 2.1:** Two phase variables in stationary reference frame [9]

$$\left[f_{\alpha\beta0}\right] = \left[T_{\alpha\beta0}\right]\left[f_{abc}\right] \tag{2.4}$$

The transformation matrix $\left[T_{\alpha\beta0}\right]$ is given by:

$$\left[T_{\alpha\beta0}\right] = \frac{2}{3}\begin{bmatrix} 1 & -\frac{1}{2} & -\frac{1}{2} \\ 0 & \sqrt{\frac{3}{2}} & -\sqrt{\frac{3}{2}} \\ \frac{1}{2} & \frac{1}{2} & \frac{1}{2} \end{bmatrix} \tag{2.5}$$

The inverse transformation is given by:

$$\left[T_{\alpha\beta0}\right]^{-1} = \begin{bmatrix} 1 & 0 & 1 \\ -\frac{1}{2} & \sqrt{\frac{3}{2}} & 1 \\ -\frac{1}{2} & -\sqrt{\frac{3}{2}} & 1 \end{bmatrix} \tag{2.6}$$

The dynamic model of the induction machine for a rotor-flux oriented vector control application can be expressed in a synchronously rotating reference frame (d-q) is given by [18]:

$$\frac{d}{dt}\begin{bmatrix} I_{sd} \\ I_{sq} \\ \psi_{rd} \\ \psi_{rq} \end{bmatrix} = \begin{bmatrix} -\left(\frac{R_s}{\sigma L_s} + \frac{{L_m}^2 R_r}{\sigma L_s {L_r}^2}\right) & \omega_e & \frac{R_r L_m}{\sigma L_s {L_r}^2} & \frac{L_m \omega_r}{\sigma L_s L_r} \\ -\omega_e & -\left(\frac{R_s}{\sigma L_s} + \frac{{L_m}^2 R_r}{\sigma L_s {L_r}^2}\right) & -\frac{L_m \omega_r}{\sigma L_s L_r} & \frac{R_r L_m}{\sigma L_s {L_r}^2} \\ \frac{R_r L_m}{L_r} & 0 & -\frac{R_r}{L_r} & \omega_{slp} \\ 0 & \frac{R_r L_m}{L_r} & -\omega_{slp} & -\frac{R_r}{L_r} \end{bmatrix} \begin{bmatrix} I_{sd} \\ I_{sq} \\ \psi_{rd} \\ \psi_{rq} \end{bmatrix} + \begin{bmatrix} \frac{U_{sd}}{\sigma L_s} \\ \frac{U_{sq}}{\sigma L_s} \\ 0 \\ 0 \end{bmatrix} \tag{2.7}$$

where: $\sigma = 1 - \frac{{L_m}^2}{L_r L_s}$

For perfect decoupling control, the total flux needs to be aligned with the d-axis, so that the q-axis rotor flux is set to zero and the d-axis rotor flux remains constant [20].

The updated model will be:

$$\frac{d}{dt}\begin{bmatrix} I_{sd} \\ I_{sq} \\ \psi_{rd} \end{bmatrix} = \begin{bmatrix} -\left(\frac{R_s}{\sigma L_s} + \frac{{L_m}^2 R_r}{\sigma L_s {L_r}^2}\right) & \omega_e & \frac{R_r L_m}{\sigma L_s {L_r}^2} \\ -\omega_e & -\left(\frac{R_s}{\sigma L_s} + \frac{{L_m}^2 R_r}{\sigma L_s {L_r}^2}\right) & \frac{L_m \omega_r}{\sigma L_s L_r} \\ \frac{R_r L_m}{L_r} & 0 & -\frac{R_r}{L_r} \end{bmatrix} \begin{bmatrix} I_{sd} \\ I_{sq} \\ \psi_{rd} \end{bmatrix} + \begin{bmatrix} \frac{U_{sd}}{\sigma L_s} \\ \frac{U_{sq}}{\sigma L_s} \\ 0 \end{bmatrix} \tag{2.8}$$

As clearly seen in equation 2.8, flux and current are coupled, i.e one affect the other. So we have to find a mechanism to make one independent of the other or simply we have to decouple them. As in [19], it is possible to update the existing model one more time, so that decoupling is succeeded.

$$\frac{d}{dt}\begin{bmatrix} I_{sd} \\ I_{sq} \\ \psi_{rd} \end{bmatrix} = \begin{bmatrix} -\left(\frac{1}{\sigma\tau_s} + \frac{1-\sigma}{\sigma\tau_r}\right) & 0 & 0 \\ 0 & -\left(\frac{1}{\sigma\tau_s} + \frac{1-\sigma}{\sigma\tau_r}\right) & 0 \\ \frac{L_m}{\tau_r} & 0 & -\frac{1}{\tau_r} \end{bmatrix} \begin{bmatrix} I_{sd} \\ I_{sq} \\ \psi_{rd} \end{bmatrix} + \frac{1}{\sigma L_s} \begin{bmatrix} {V_{sd}}^* \\ {V_{sq}}^* \\ 0 \end{bmatrix} \tag{2.9}$$

where: $\tau_r = \frac{L_r}{R_r}, \quad \tau_s = \frac{L_s}{R_s}, \quad {V_{sd}}^* = U_{sd} - {V_{sd}}^{dcpl}, \quad {V_{sq}}^* = U_{sq} - {V_{sq}}^{dcpl}$

$$\begin{bmatrix} V_{sd}^{dcpl} \\ V_{sq}^{dcpl} \end{bmatrix} = \begin{bmatrix} w_e I_{sq} + \frac{L_m}{\sigma L_s L_r \tau_r}\psi_{rd} \\ -w_e I_{sd} - \frac{L_m}{\sigma L_s L_r \tau_r}\psi_{rd} \end{bmatrix} \tag{2.10}$$

And the electromagnetic torque equation becomes:

$$T_e = \frac{3}{2}\frac{p}{2}\frac{L_m}{L_r}\psi_r I_{sq} \tag{2.11}$$

Where p is number of poles.

## 2.3 Control Methods of Induction Motor

The speed or position control and estimation of AC machine drives are more complex than DC drives. This complexity exacerbates substantially if high performance is in need. This complexity arises from the need of variable frequency drive, harmonically optimum converter power supplies and in addition, complex dynamics of AC machines, machine parameter variations and the difficulties of processing feedback signals in the presence of harmonics [4].

**Scalar speed control**

As the name indicates, it takes into account only magnitude variations and coupling effect is not considered. Compared with vector control (to be discussed in a while) where both magnitude and phase are controlled, it is some what inferior in performance, although easy to implement. Scalar controlled motors widely used in industries. However their need is highly diminished due to superior performance of vector control. Vector control (Field oriented control) has been implemented to manage the shortcomings of the scalar [14].

**Field Oriented Control**

Vector control, also called Field oriented control (FOC), is a variable frequency drive (VFD) control method. The stator currents of a three phase induction motor are transformed to a two orthogonal components. This technique decouples the transformed components of stator current space vector: one providing the control of flux and the other providing the control of torque. The two components are defined in the synchronously rotating reference frame. With the help of this control technique the induction motor can replace a separately excited DC motor. The scalar control technique is easier to implement, but as stated above, it has the coupling effect which is responsible for the sluggish response, this leads to instability due to higher order system effect. The main effort is to replace DC motor by an induction motor and merge the advantages of both the motors together into variable speed brush-less motor drive and eliminate the associated problems [35].

Variable speed or adjustable torque control of electrical motor drives are crucial components in almost all modern industrial manufacturing processes. The best part of field oriented control is, it decouples the torque and flux components of the machine by multiple co-ordinate transformation, with a suitable modulator to generate switching pulses for the power converter to control the machine. For all above mentioned reasons, this method provides very fast dynamics in speed control loop [3]. These days field oriented control (FOC) are the best performing methods [15, 35] . FOC is more advanced control method widely utilized in the algorithm of induction motor driving system.

FOC method is widely used for three-phase electric drive systems [11]. Using this method, we can get three-phase AC motors acting similar to separately excited DC motors (create flux and generate torque). Classical structure of field-oriented control for three-phase AC drives using induction motor need a speed sensor such as shaft encoder for speed control. But installation of encoders is difficult and costly. Likewise, this method with a flux estimator does not work in a low speed region well, because it is very sensitive to the offset of the voltage sensor and stator resistance variation. So sensor-less field oriented control can overcome the stated drawbacks. Advantages of sensor-less field oriented control are Improved torque response, Reduction in size of motor and cost, Reduction in power consumption and Dynamic speed accuracy[35].

**Principles of Field Oriented Control**

There are two approaches to get the flux vector, direct field oriented control(DFOC) and indirect field oriented control(IFOC). The two methods differ in the way the rotor position is determined. In

direct FOC the rotor flux position is directly measured from the air gap flux using a suitable sensors or deduced from integration of the back EMF, while in indirect FOC, the rotor flux position is obtained from slip speed computation. The major weakness of IFOC approach is, it is centered upon the accuracy of the control gains which, in turn, depend to a great extent on the motor parameters assumed in the feed forward control algorithm [35].

As stated in [20] the indirect field-oriented control is sensitive to some uncertain parameters. It is give by:

$$\theta_e = \int (\omega_{slp} + \omega_r) dt \tag{2.12}$$

where $\theta_e$ and $\omega_r$ are rotor flux position and rotor speed respectively.

As stated in the [38] structure of direct rotor magnetic field oriented FOC uses two closed loops: the first loop is fed back by rotor flux linkage and direct axis current, and the other loop is fed back by the rotor speed and quadrature axis current. Therefore, the accurate acquisition of the rotor flux linkage and velocity guarantee the excellent performance of Direct FOC drive. So this method is chosen for this thesis.

## 2.4 Controller Design

Induction motor dynamic model based controller can be designed from equation 2.9. Transforming equation 2.9 to the block diagram, as in figure 2.2.

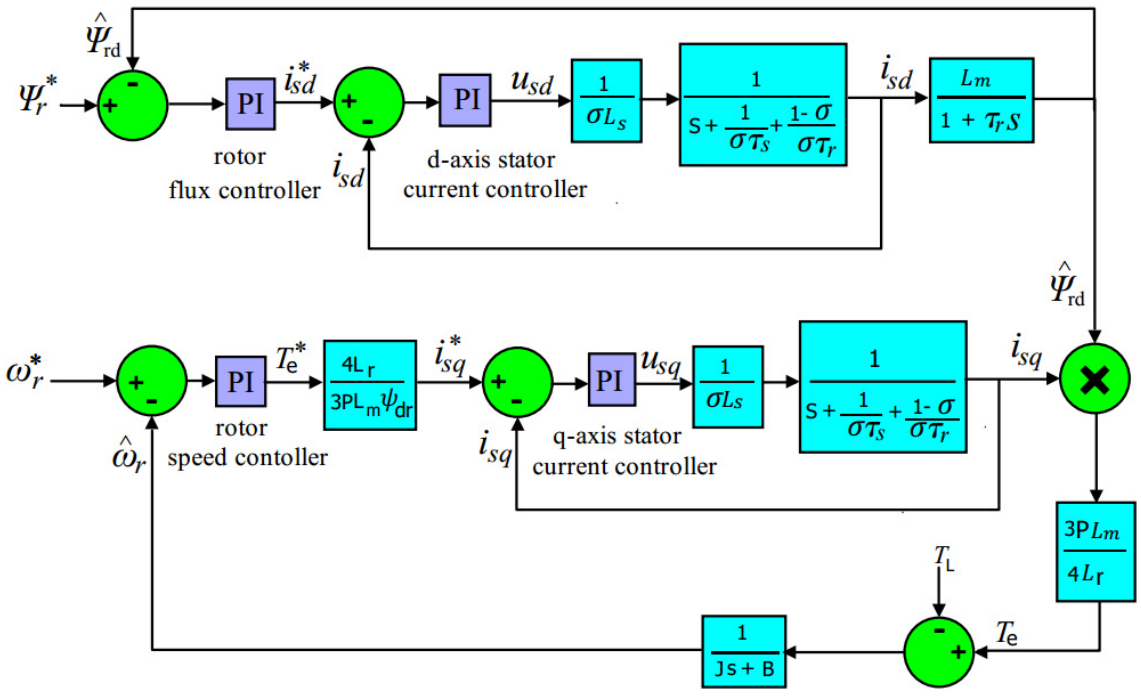


**Figure 2.2:** Model based induction motor drives[19]

$\psi_{rd}$ is rotor flux obtained from measured motor current model and $i_{sq}$ is q-current measured from the motor model. The transfer function of the plant for the controllers of the vector controlled induction motor drives can be derived as follows [19].

For the d-axis current controller designing as clearly seen $U_{sd}$ is an input and $I_{sd}$ is output to the

corresponding part of plant as shown in figure 2.2. Using the above stated concept the controller can be designed as follows:

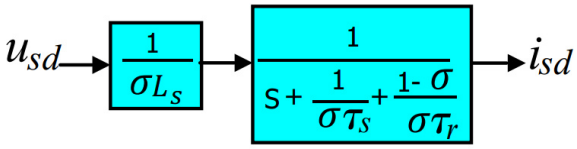


**Figure 2.3:** D-axis current controller block

Let the transfer function from $U_{sd}$ to $I_{sd}$ be $G_{id}(s)$ : then

$$G_{id}(s) = \frac{I_{sd}}{U_{sd}} = \frac{\frac{1}{\sigma L_s}}{s+\frac{1}{\sigma\tau_s}+\frac{1-\sigma}{\sigma\tau_r}} = \frac{\frac{1}{\sigma L_s}}{s+\frac{\tau_s+\tau_r-\sigma\tau_s}{\sigma\tau_s\tau_r}} \tag{2.13}$$

For q-axis current controller :

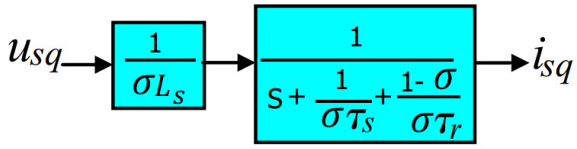


**Figure 2.4:** Q-axis current controller block

$$G_{Iq}(s) = \frac{I_{sq}}{U_{sq}} = \frac{\frac{1}{\sigma L_s}}{s+\frac{1}{\sigma\tau_s}+\frac{1-\sigma}{\sigma\tau_r}} = \frac{\frac{1}{\sigma L_s}}{s+\frac{\tau_s+\tau_r-\sigma\tau_s}{\sigma\tau_s\tau_r}} \tag{2.14}$$

For rotor flux controller :

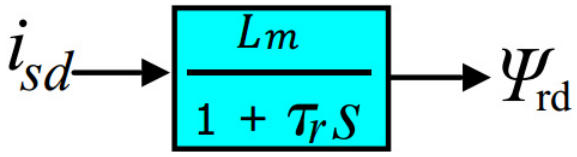


**Figure 2.5:** Rotor flux controller block

$$G_{flx}(s) = \frac{\Psi_{rd}}{I_{sd}} = \frac{\frac{L_m}{\tau_r}}{s+\frac{1}{\tau_r}} \tag{2.15}$$

For speed controller :

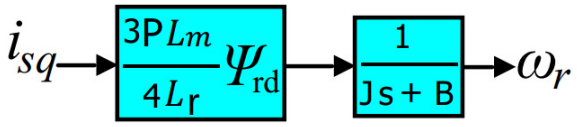


**Figure 2.6:** Speed controller block

$$G_{\omega_r}(s) = \frac{\omega_r}{I_{sq}} = \frac{\frac{k}{J_m}}{s + \frac{B}{J_M}} \quad where: k = \frac{3PL_m\psi_{rd}}{4L_r} \tag{2.16}$$

The transfer function of current is give by:

$$G_I(s) = \frac{I_s}{V_s} = \frac{\frac{1}{\sigma L_s}}{s + \frac{1}{\sigma\tau_s} + \frac{1-\sigma}{\sigma\tau_r}} = \frac{\frac{1}{\sigma L_s}}{s + \frac{\tau_s+\tau_r-\sigma\tau_s}{\sigma\tau_s\tau_r}} \tag{2.17}$$

$$C(s) = k_p + \frac{k_i}{s} \tag{2.18}$$

After some rearrangement the PI controller will be

$$C(s) = \frac{k_p\left(s + \frac{k_i}{k_p}\right)}{s} \tag{2.19}$$

$$G_I(s)C(s) = \frac{\frac{1}{\sigma L_s}}{s + \frac{\tau_s+\tau_r-\sigma\tau_s}{\sigma\tau_s\tau_r}} * \frac{k_p\left(s + \frac{k_i}{k_p}\right)}{s} \tag{2.20}$$

Applying a pole-zero cancellation to equation 2.20

$$\frac{k_i}{k_p} = \frac{\tau_s + \tau_r - \sigma\tau_s}{\sigma\tau_s\tau_r} \tag{2.21}$$

$$k_p = BW.\sigma L_s \tag{2.22}$$

$$k_i = \frac{\tau_s + \tau_r - \sigma\tau_s}{\sigma\tau_s\tau_r}.BW.\sigma L_s \tag{2.23}$$

where BW, bandwidth of the controller.

All the above computed controllers are in continuous time domain. But for real time applications, they all must be converted to discrete time domain.

Controller design in discrete time domain involves some steps. First calculating the open loop transfer function of the plant, then deriving the loop gain of the control system using a pole-zero cancellation method and finally deducing the parameters of the controller for the specified bandwidth.

Block diagram of the current controller in discrete time domain is given in figure 2.7.

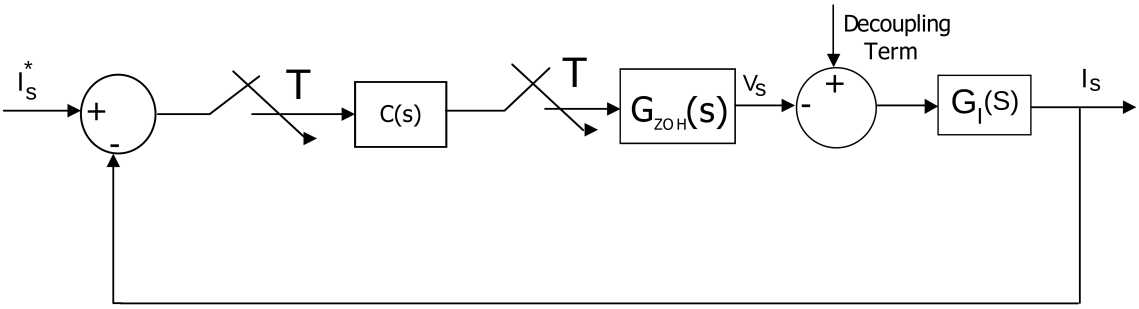


**Figure 2.7:** Current controller block-diagram [19]

PI controller in discrete form for T sampling time:

STEP 1: The open loop transfer function of the plant in discrete time domain can be computed as follows: Applying Z-transfom (backward Euler) to equation 2.18

$$C(z) = k_p + \frac{k_i T z}{z-1} \tag{2.24}$$

After some rearrangement equation 2.24 will be

$$C(z) = \frac{(k_p + k_i T)z - k_p}{z-1} \tag{2.25}$$

$$G_{ZOH} = \frac{1-\exp(-T)}{s} \tag{2.26}$$

$$\frac{I_s(z)}{\Delta I_s(z)} = C(z).Z[G_{ZOH}(s).G_I(s)] \tag{2.27}$$

$$\frac{I_s(z)}{\Delta I_s(z)} = \frac{(k_p + k_i T)\tau_r \tau_s}{L_s(\tau_r + \tau_s - \sigma\tau_s)} . \frac{(z - \frac{k_p}{k_p + k_i T})[1 - \exp(-\frac{\tau_r + \tau_s - \sigma\tau_s}{\sigma\tau_r\tau_s} T)]}{(z-1)[z - \exp(-\frac{\tau_r + \tau_s - \sigma\tau_s}{\sigma\tau_r\tau_s})]} \tag{2.28}$$

STEP 2: Deriving the loop gain of the control system using a pole-zero cancellation method.

$$\frac{k_p}{k_p + k_i T} = \exp(-\frac{\tau_r + \tau_s - \sigma\tau_s}{\sigma\tau_r\tau_s}) \tag{2.29}$$

writing $k_p$ interms of $k_i$:

$$k_p = \frac{\exp(-\frac{\tau_r + \tau_s - \sigma\tau_s}{\sigma\tau_r\tau_s} T).k_i T}{1 - \exp(-\frac{\tau_r + \tau_s - \sigma\tau_s}{\sigma\tau_r\tau_s} T)} \tag{2.30}$$

Substituting equation 2.29 into equation 2.28:

$$\frac{I_s(z)}{\Delta I_s(z)} = \frac{(k_p + k_i T)\tau_r \tau_s}{L_s(\tau_r + \tau_s - \sigma\tau_s)} . \frac{\left(1 - \exp(-\frac{\tau_r + \tau_s - \sigma\tau_s}{\sigma\tau_r\tau_s} T)\right)}{(z-1)} \tag{2.31}$$

STEP 3:

Deducing the parameters of the controller for the specified bandwith:

The closed loop transfer function is

$$\frac{I_s(z)}{I^*{}_s(z)} = \frac{\frac{(k_p+k_iT)\tau_r\tau_s\left(1-\exp(-\frac{\tau_r+\tau_s-\sigma\tau_s}{\sigma\tau_r\tau_s}T)\right)}{L_s(\tau_r+\tau_s-\sigma\tau_s)}}{z-1+\frac{(k_p+k_iT)\tau_r\tau_s\left(1-\exp(-\frac{\tau_r+\tau_s-\sigma\tau_s}{\sigma\tau_r\tau_s}T)\right)}{L_s(\tau_r+\tau_s-\sigma\tau_s)}} \tag{2.32}$$

The bandwidth of the first order system is given with its corresponding representation in discrete time-domain is [19]:

$$Z[G_{ZOH}(S)\frac{BW}{s+BW}] = \frac{1-\exp(-BW.T)}{z-\exp(-BW.T)} \tag{2.33}$$

Comparing equation 2.32 and 2.33 results in:

$$k_p + k_iT = \frac{[1-\exp(-BW.T)]L_s(\tau_r+\tau_s-\sigma\tau_s)}{\tau_r\tau_s\left(1-\exp(-\frac{\tau_r+\tau_s-\sigma\tau_s}{\sigma\tau_r\tau_s}T)\right)} \tag{2.34}$$

Substituting equation 2.30 into equation 2.34:

$$k_i = \frac{[1-\exp(-BW.T)]L_s(\tau_r+\tau_s-\sigma\tau_s)}{\tau_r\tau_sT} \tag{2.35}$$

$$k_p = \frac{\exp\left(-\frac{\tau_r+\tau_s-\sigma\tau_s}{\sigma\tau_r\tau_s}T\right)[1-\exp(-BW.T)]L_s(\tau_r+\tau_s-\sigma\tau_s)}{\tau_r\tau_s\left(1-\exp(-\frac{\tau_r+\tau_s-\sigma\tau_s}{\sigma\tau_r\tau_s}T)\right)} \tag{2.36}$$

With the same procedure flux controller gains :

$$k_i = \frac{1-\exp(-BW.T)}{L_mT} \tag{2.37}$$

$$k_p = \frac{\exp\left(-\frac{1}{\tau_r}T\right)[1-\exp(-BW.T)]}{\left(1-\exp(-\frac{1}{\tau_r}T)\right)L_m} \tag{2.38}$$

Speed controller gains :

$$k_i = \frac{[1-\exp(-BW.T)]B_m}{T} \tag{2.39}$$

$$k_p = \frac{\exp\left(-\frac{B_m}{J_m}T\right)[1-\exp(-BW.T)]B_m}{\left(1-\exp\left(-\frac{B_m}{J_m}T\right)\right)} \tag{2.40}$$

## 2.5 Space Vector Pulse Width Modulation

Space Vector PWM (SVPWM) refers to a special technique of determining the switching sequence of the upper three power transistors of a three-phase voltage source inverter (VSI). In power electronic converters, the electrical energy frequency is converted from one level of voltage/current/ into another using semiconductor-based electronic switch. Application areas of power electronic

converters are improved much in semiconductor technology, they offer higher voltage and current ratings as well as better switching characteristics. The main advantages of modern power electronic converters are higher efficiency, less weight, smaller dimensions, fast operation, and higher-power densities. The switches are operated only in one of two states, either fully ON or OFF, unlike other types of electrical circuits where the control elements are operated in a linear active region. This is the best characteristics of these types of circuits. There are many modulation techniques available now a days, but the SVPWM technique is the most popular technique due to its efficient DC bus voltage use and easy implementation [1]. To reduce the harmonic contents in the inverter output, SVPWM based Voltage source inverter circuit is a best choice. In this method, a revolving reference vector is used to provide the reference voltage. The voltage magnitude as well as the frequency of the reference vector are used to efficiently control both the line voltage magnitude as well as the line frequency. Thus, the effective THD can be minimized by the introduction of this control technique at the inverter side [14].

The idea of the SVPWM relies on depiction of the inverter output voltage as space vectors. Space vector depiction of the output voltages of the inverter is realized for the implementation of SVPWM. Space vector at the same time represent three-phase quantities as one rotating vector, therefore each phase is not considered on an individual basis. The three phases are taken as only one quantity. The space vector depiction is valid for both transient and steady state conditions in contrast to phasor representation, which is valid only for steady state conditions. The rotating air-gap MMF in a three-phase induction machine brought the concept of space vector. By supplying balanced three-phase voltages to the three-phase balanced winding of a three-phase induction machine, rotating MMF is produced, which rotates at the same speed as that of individual voltages, with an amplitude of $\frac{3}{2}$ times the individual voltage amplitude [1].

SVPWM is a relatively new and popular technique in controlling motor devices. In the space vector PWM method, the output voltage is approximated using the nearest three output vectors that the nodes of the triangle containing the reference vector in the space vector diagram of the inverter. When the reference vector changes from one region to another, it may induce an abrupt change in the output vector. In addition we need to calculate the switching sequences and time of the states at every change of the reference voltage location. The space vector is defined as [1]:

$$f_s = \frac{2}{3}\left[f_a + e^{i\frac{2\pi}{3}} f_b + e^{i\frac{4\pi}{3}} f_c\right] \tag{2.41}$$

where: $f_a, f_b, f_c$ could be three phase voltage,current or flux quantities.

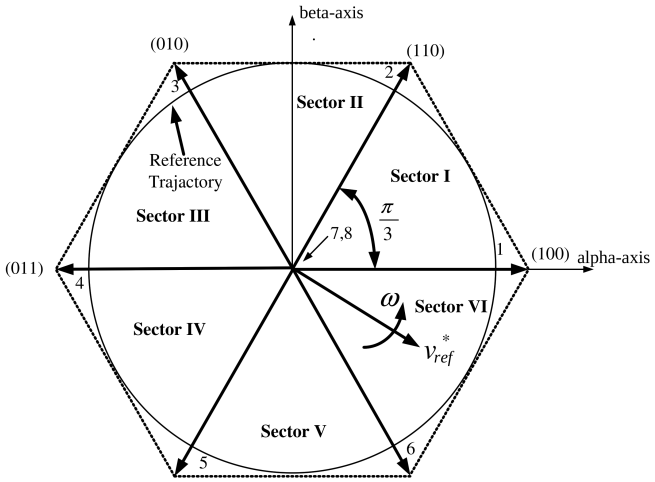


**Figure 2.8:** Voltage space vector locations corresponding to different switching states [1]

A circle inscribed inside the state map corresponds to sinusoidal operation. The area inside the inscribed circle is called the linear modulation region or under-modulation region. As seen in Figure 2.8, the area between the inside and outside circle of the hexagon is called the nonlinear modulation region or over-modulation region. The concepts in the operation of linear and nonlinear modulation regions depend on the modulation index, which reflects on the inverter utilization capability.

The Space vector pulse width modulation technique has the following some additional advantages, such as third-harmonic injection ability, better DC-link utilization and less commutation losses as it prevents unnecessary switching.

## 2.6 Implementation of space vector PWM

The target of the SVPWM control of the inverter switches is to synthesize the desired reference stator voltage space vector in an optimum manner with objectives of constant switching frequency fs, Smallest instantaneous deviation from its reference value and Maximum utilization of the available dc-bus voltage.

The relationship between the switching function and the phase voltage is given by [32]:

$$\begin{bmatrix} V_{an} \\ V_{bn} \\ V_{cn} \end{bmatrix} = \frac{V_{dc}}{3} \begin{bmatrix} 2 & -1 & -1 \\ -1 & 2 & -1 \\ -1 & -1 & 2 \end{bmatrix} \begin{bmatrix} T_a \\ T_b \\ T_c \end{bmatrix} \tag{2.42}$$

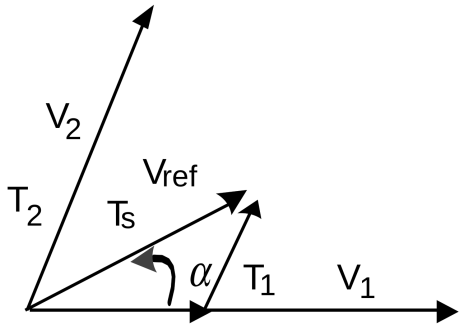


**Figure 2.9:** Voltage space vector locations corresponding to different switching states [9]

SVPWM implementation procedures :

- Determine angle $(\alpha)$ and reference voltage $V_{ref}$ from the input voltage components.
- Determine the sectors.
- Determine the adjacent space vectors $V_1$ and $V_2$.
- Determine time duration $T_a, T_b, T_0$ using sampling time and angle $(\alpha)$ .
- Determine the switching time duration at any sector.

Step 1 : In the SVPWM, the three phase output voltage vector is represented by a reference vector that rotates at an angular speed of $\omega = 2\pi f$. The SVPWM uses the combinations of switching states to approximate the reference vector. A reference voltage vector ( $V_{ref}$ ) that rotates with angular speed in the plane represents three sinusoidal wave forms with angular frequency in the coordinate system. The three phase voltages could be described with only two components and in a two dimensional plane. The magnitude of each active vector is $\frac{2V_{dc}}{3}$. The active vectors are indicated by the hexagon boundary. The locus of the circle projected by the space reference vector depends on the occurrence of 8 possibilities. i.e $2^3 = 8$ of which 2 are idle, i.e $(000)$ and $(111)$ as indicated on the figure 2.9.
In stationary reference frame $V_{s\alpha}$ and $V_{s\beta}$ are given as [24]:

$$\begin{bmatrix} V_{s\alpha} \\ V_{s\beta} \end{bmatrix} = \frac{2}{3} \begin{bmatrix} 1 & -\frac{1}{2} & -\frac{1}{2} \\ 0 & \frac{\sqrt{3}}{2} & -\frac{\sqrt{3}}{2} \end{bmatrix} \begin{bmatrix} V_{an} \\ V_{bn} \\ V_{cn} \end{bmatrix} \tag{2.43}$$

From equation 2.43 we can determine $V_{ref}$ and $angle(\alpha)$ ,then :

$$|V_{ref}| = \sqrt{{V_{s\alpha}}^2 + {V_{s\beta}}^2} \tag{2.44}$$

$$\alpha = \tan^{-1}\left(\frac{V_{s\beta}}{V_{s\alpha}}\right) \tag{2.45}$$

Step 2 : The process of switching the electronic devices in a power electronic converter from one state to another is called 'modulation'. The modulation index (MI) shows the mode of operation i.e under modulation or over modulation. In order to determine the modulation index we have to first

determine the fundamental peak value of the square phase voltage wave i.e $\frac{2V_{dc}}{\pi}$. The modulation index can be express as [24]:

$$MI = \frac{V_{ref}}{V_{\max\_six\_step}} \tag{2.46}$$

### Sector number determination

Determination of switching time and sequence, is sector knowledge dependent. So based on the position of reference vector there are eight switching states, but only six are active. Two active or idle states at a time are not allowed.

**Table 2.1:** Sector number determination

| sector | angle |
|---|---|
| 1 | $0^\circ < \alpha \leq 60^\circ$ |
| 2 | $60^\circ < \alpha \leq 120^\circ$ |
| 3 | $120^\circ < \alpha \leq 180^\circ$ |
| 4 | $180^\circ < \alpha \leq 240^\circ$ |
| 5 | $240^\circ < \alpha \leq 300^\circ$ |
| 6 | $300^\circ < \alpha \leq 360^\circ$ |

### Duty cycle determination

As in [1], the duty cycle of the different space vectors are calculated using the 'equal volt -second principle'. It states, the product of the reference voltage and the switching time must be equal to the product of the applied voltage vectors and their duty cycles, with assumption that the reference voltage remains fixed during the switching interval. When the reference voltage is in sector I, the reference voltage can be synthesized by using the vectors $V_a, V_b$, and $V_0$ (zero vector), applied for time $T_a, T_b$, and $T_0$ respectively. Hence, using the equal volt-second principle, for sector I

$$V_{ref}T_s = V_1T_1 + V_2T_2 + V_0T_0 \tag{2.47}$$

$$T_s = T_1 + T_2 + T_0 \tag{2.48}$$

The space vectors are given as:

$$V_{ref} = \left|V_{ref}\right| e^{i\alpha}, \quad V_1 = \frac{2}{3}V_{dc}e^{i0}, \quad V_2 = \frac{2}{3}V_{dc}e^{i\frac{\pi}{3}}, \quad V_0 = 0 \tag{2.49}$$

substituting equations 2.49 into equation 2.47

$$\left|V_{ref}\right| e^{i\alpha}T_s = \frac{2}{3}V_{dc}e^{i0}T_1 + \frac{2}{3}V_{dc}e^{i\frac{\pi}{3}}T_2 \tag{2.50}$$

Expanding equation 2.50 then, separating real and imaginary part results in the following equations.

$$T_s\left|V_{ref}\right|\cos\alpha = T_1\frac{2}{3}V_{dc} + T_2\frac{2}{3}V_{dc}\cos\left(\frac{\pi}{3}\right) \tag{2.51}$$

$$T_s \left|V_{ref}\right| \sin\alpha = T_2 \frac{2}{3} V_{dc} \sin\left(\frac{\pi}{3}\right) \tag{2.52}$$

where:

$$[0^\circ \leq \alpha \leq 60^\circ]$$

Solving for $T_1, T_2$ and $T_0$ from equation 2.51 , 2.52 and 2.48:

$$T_0 = \frac{\sqrt{3}T_s}{2V_{dc}}\left(-\sqrt{3}V_\alpha + V_\beta\right), \quad T_1 = \frac{\sqrt{3}T_s}{2V_{dc}}\left(\sqrt{3}V_\alpha - V_\beta\right), \quad T_2 = \frac{\sqrt{3}T_s}{V_{dc}}V_\beta$$

**Determine the switching time of each transistor ($S_1$ to $S_6$)**

In space vector PWM implementation, there are many alternatives for switching patterns, It should be arranged in such a way that switching losses are minimum. So the suggested way is, the two adjacent active vectors and two zero vectors are used in each sector. So for proper implementation every single switching period starts with one zero vector and end with another zero vector during the sampling time.

**Table 2.2:** Switching time of each transistor

| Sector | Upper switches($S_1, S_3, S_5$) | Lower switches($S_4, S_6, S_2$) |
|---|---|---|
| 1 | $S_1 = \frac{T_0}{4} + T_1 + \frac{T_2}{2}$<br>$S_3 = \frac{T_0}{4} + T_2$<br>$S_5 = \frac{T_0}{4}$ | $S_4 = \frac{T_0}{4}$<br>$S_6 = \frac{T_0}{4} + T_1$<br>$S_2 = \frac{T_0}{4} + T_1 + \frac{T_2}{2}$ |
| 2 | $S_1 = \frac{T_0}{4} + T_1$<br>$S_3 = \frac{T_0}{4} + T_1 + \frac{T_2}{2}$<br>$S_5 = \frac{T_0}{4}$ | $S_4 = \frac{T_0}{4} + T_2$<br>$S_6 = \frac{T_0}{4}$<br>$S_2 = \frac{T_0}{4} + T_1 + \frac{T_2}{2}$ |
| 3 | $S_1 = \frac{T_0}{4}$<br>$S_3 = \frac{T_0}{4} + T_1 + \frac{T_2}{2}$<br>$S_5 = \frac{T_0}{4} + T_2$ | $S_4 = \frac{T_0}{4} + T_1 + \frac{T_2}{2}$<br>$S_6 = \frac{T_0}{4}$<br>$S_2 = \frac{T_0}{4} + T_1$ |
| 4 | $S_1 = \frac{T_0}{4}$<br>$S_3 = \frac{T_0}{4} + T_1$<br>$S_5 = \frac{T_0}{4} + T_1 + \frac{T_2}{2}$ | $S_4 = \frac{T_0}{4} + T_1 + \frac{T_2}{2}$<br>$S_6 = S_1 = \frac{T_0}{4} + T_1$<br>$S_2 = \frac{T_0}{4}$ |
| 5 | $S_1 = \frac{T_0}{4} + T_1$<br>$S_3 = \frac{T_0}{4}$<br>$S_5 = \frac{T_0}{4} + T_1 + \frac{T_2}{2}$ | $S_4 = \frac{T_0}{4} + T_1$<br>$S_6 = \frac{T_0}{4} + T_1 + \frac{T_2}{2}$<br>$S_2 = \frac{T_0}{4}$ |
| 6 | $S_1 = \frac{T_0}{4} + T_1 + \frac{T_2}{2}$<br>$S_3 = \frac{T_0}{4}$<br>$S_5 = \frac{T_0}{4} + T_1$ | $S_4 = \frac{T_0}{4}$<br>$S_6 = \frac{T_0}{4} + T_1 + \frac{T_2}{2}$<br>$S_2 = \frac{T_0}{4} + T_1$ |

## 2.7 Inverter

Inverter is the power electronic circuit, which converts the DC voltage into AC one. The output voltage can be controlled with the help of drives of the switches. The pulse width modulation

techniques are most commonly used to control the output voltage of inverters. Such inverters are called as PWM inverters. Inverters can be broadly classified into Voltage Source Inverter (VSI) and Current Source Inverter (CSI).

When the DC voltage remains constant, then it is called Voltage Source Inverter (VSI) or Voltage Fed Inverter (VFI). When input current is maintained constant, then it is called Current Source Inverter (CSI) or Current Fed Inverter (CFI). Some times, the DC input voltage to the inverter is controlled to adjust the output. Such inverters are called Variable DC Link Inverters. Inverters are used in variable frequency AC motor drives.

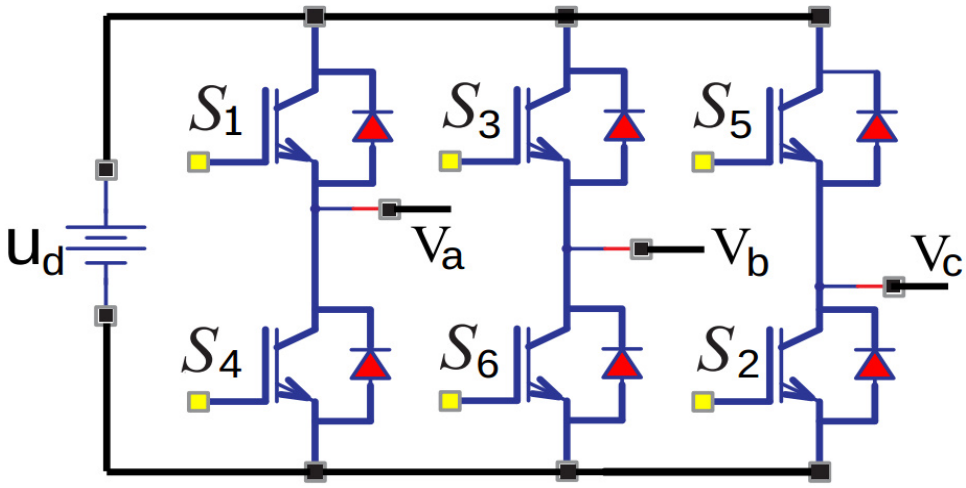


**Figure 2.10:** Two-level inverter [8]

**Table 2.3:** VSI and CSI comparison

| VSI | CSI |
|---|---|
| VSI is fed from a DC voltage source having small or negligible impedance. | CSI is fed with adjustable current from a DC voltage source of high impedance. |
| Input voltage is maintained constant | The input current is constant but adjustable. |
| Output voltage does not dependent on the load. | The amplitude of output current is independent of the load. |
| VSI requires feedback diodes. | The CSI does not require any feedback diodes. |
| The commutation circuit is complicated | Commutation circuit is simple as it contains only capacitors. |
| Power BJT, Power MOSFET, IGBT, GTO with self commutation can be used in the circuit. | They cannot be used as these devices have to withstand reverse voltage. |

# 3 Model Reference Adaptive System and Luenberger Observer

## 3.1 Induction Motor Speed Estimation Methods

Many induction motor speed estimation methods are proposed in different literature, some of them are discussed as follows.

**Slip calculation**

Rotor speed can be determined from slip speed $\omega_{slp}$ using the relation $\omega_r = \omega_e - \omega_{slp}$.
slip speed is given by [4]:

$$\omega_{slp} = \frac{(1+\sigma s\tau_r)\, L_s i_{sq}}{\tau_r\,(\psi_{sd} - \sigma L_s i_{sd})} \tag{3.1}$$

For indirect field oriented control $\omega_e$ signal can be obtained directly as a control variable. For high efficiency machines, near synchronous speed, accurate computation of slip speed is difficult, as the signal magnitude is small and dependent on machine parameter. In addition direct integration of machine terminal voltages at low speed bring up a problem to synthesize $\omega_{slp}$ and $\omega_e$ signals.

**Direct synthesis from state equations**

The stationary $\alpha$-$\beta$ reference frame dynamic equations of a machine can be rearranged to figure out the rotor speed directly [14].

$$\theta_e = \arctan\left(\frac{\psi_{r\beta}}{\psi_{r\alpha}}\right) \tag{3.2}$$

Differentiating 3.2 results in:

$$\omega_r = \frac{d\theta_e}{dt} - \omega_{slp} \tag{3.3}$$

This method similar with slip calculation method. This synthesis method is highly parameter dependent and it gives poor accuracy of estimation.

**Model reference adaptive system(MRAS)**

As in [16, 13, 12] rotor speed can be computed by the Model Reference Adaptive Systems (MRAS), where the response of the a reference model (voltage model) is compared with the response of the adjustable or adaptive model (current model) until the errors between the two models approach to zero. In practical implementation the rotor flux synthesis based on voltage model is difficult, in

particular at low speed, pure integration of the voltage signal is still problem[4]. Model Reference Adaptive System (MRAS) speed estimation algorithm is still valid if, instead of pure integration, the corresponding back EMF signals are compared through some low pass filter. However, error of estimation due to parameter variation at low speed exacerbates. The detail will be discussed in section 3.4.

**Speed adaptive flux observer(Luenberger observer)**

As in [21, 18, 17, 23, 4] speed adaptive flux observer works as the name indicates, the flux will be observed from the reference model and speed will be adapted in adjustable model and associated to work as model reference adaptive system. An observer is an estimator that uses a plant model (partial or full) and a feedback loop with measured plant variables. Gain G (Luenberger gain) is used to take care of current or flux estimation part and Lyapunov's direct stability analysis is used to drive the speed adaptation algorithm. Although estimation accuracy is highly improved by Luenberger observer, parameter variation is still the headache (particularly rotor and stator resistance). The estimation accuracy is low as the speed gets closer to zero.

**Extended Kalman filter**

As stated in [33, 18, 36] the extended kalman filter (EKF) is a full order stochastic observer for the recursive optimum state estimation of a non-linear dynamical system in real time using signal that are corrupted by noise . The statistics of noise and measurements are given by 3 covariance matrices : Q, R and P where Q is system noise vector covariance matrix $5x5$, R is measurement noise vector covariance matrix $2x2$, and P is system state vector covariance matrix $5x5$. So computation of the stated matrices is complex. Due to its high complexity and high computation time, even with a powerful DSP, it takes much time and difficult to apply in real time, particularly for fast speed variations. In addition parameter variation is still a problem that makes accuracy poor at low speeds.

## 3.2 Luenberger Observer

As in [36] Luenberger Observer (deterministic) was first introduced by David G. Luenberger, it is an improvement of rotor speed estimation that operates on the principle of a speed adaptive flux observer. Observers those are dependent on induction motor model, have accuracy problems at low speed. For non-linear systems (in this case induction motor), the Luenberger Observer can be used to observe the rotor flux. Luenberger observer uses induction motor model and a feedback loop with measured stator current and rotor flux. The observer gain matrix must be designed based on Lyapunov's asymptotic stability theory, and the observer must be faster than the observed system. Luenberger speed estimator is the most attractive approach, due to its design simplicity [5]. The principle of Luenberger observer consists in duplicating the real system and in correction of its state based on the real system output feedback [15]. This observer is used to estimate the rotor flux components and rotor speed of induction motor by including an adaptive mechanism based on the Lyapunov's stability theory [11]. Generally, the equations of the Luenberger Observer can be

expressed as follow [10].

$$\begin{cases} \hat{\dot{x}} = A\hat{x} + Bu + G(y - \hat{y}) \\ \hat{y} = c\hat{x} \end{cases} \tag{3.4}$$

where the symbol ˆ denotes estimated values and G is the Luenberger gain matrix. A is state matrix, B is input matrix, C is output matrix, u is input, y is measured output, and x is state vector of the system. To ensure stability in all speed ranges, the trend is to select the observer poles proportional to the motor poles (the proportionality constant is $k > 1$). If the poles of the induction motor are given by $\lambda_{IM}$, the observer poles $\lambda_{LO}$ are selected as: $\lambda_{LO} = k * \lambda_{IM}$ . To ensure that the estimation error vanishes over time, we should select the observer gain matrix G so that $(A - GC)$ is asymptotically stable. Hence, the observer gain matrix should be chosen so that all eigenvalues of (A-GC) have negative real parts [18].

**Stater Current Based Luenberger Observer Design**

Luenberger Observer replaces the most widely used voltage model of the induction motor as it replicates the whole system and calculates all variables. Further, the states of the system are corrected through the negative feedback of the comparison between the original system and the observer output. Usually, the input of the system is voltage vector, state variables are currents and rotor flux and output is also the current [23]. Stator and rotor flux estimation is one of the crucial factor that determines the stability and dynamic performance of the drives operation [22]. The stator voltage equation can be expressed as [29]:

$$V_s = R_s i_s + \frac{d\psi_s}{dt} + U_{comp} \tag{3.5}$$

Or

$$\psi_s = \int (V_s - R_s i_s - U_{comp}) dt \tag{3.6}$$

where $U_{comp}$ is compensation for disturbances like offsets, unbalances, and errors in the estimated induced voltage. The errors are resulting from either the voltage signal or from the current signal, and the major source of error is a mismatch of the model parameter .
Rearranging equation 3.5 :

$$i_s = \frac{V_s - \frac{d\psi_s}{dt} - U_{comp}}{R_s} \tag{3.7}$$

The stator and rotor flux linkage is given by the following well known equations.

$$\psi_s = L_s i_s + L_m i_r \tag{3.8}$$

$$\psi_r = L_r i_r + L_m i_s \tag{3.9}$$

Rearranging equation 3.9:

$$i_r = \frac{\psi_r - L_m i_s}{L_r} \tag{3.10}$$

Substituting equation 3.10 in to equation 3.8 results in:

$$\psi_s = L_s i_s + L_m \left( \frac{\psi_r - L_m i_s}{L_r} \right) \tag{3.11}$$

Rearranging equation 3.11:

$$\psi_s = \frac{L_m}{L_r} \psi_r + \left( L_s - \frac{{L_m}^2}{L_r} \right) i_s \tag{3.12}$$

Substituting equation 3.7 into equation 3.12

$$\psi_s = \frac{L_m}{L_r} \psi_r + \left( L_s - \frac{{L_m}^2}{L_r} \right) \left( \frac{V_s - \frac{d\psi_s}{dt} - U_{comp}}{R_s} \right) \tag{3.13}$$

After some rearrangement equation 3.13 becomes as in [16, 20]:

$$\frac{d\hat{\psi}_s}{dt} = \frac{1}{\sigma \tau_s} (-\hat{\psi}_s + k_r \hat{\psi}_r) + V_s - U_{comp} \tag{3.14}$$

where : $k_r = \frac{L_m}{L_r}$ $U_{comp} = G(i_s - \hat{i}_s)$ or $U_{comp} = G'(\psi_s - \hat{\psi}_s)$
To correct the estimated stator flux deviation, to compensate error arising from pure integrator at low speed and to provide a wide speed range operation of the observer, the voltage model is adapted through a PI compensator [29, 30, 25, 20]:

$$U_{comp} = \left[ K_p + \frac{K_p}{T_I} \int_0^t d\tau \right] \left( {\psi^v}_s - {\psi^i}_s \right) \tag{3.15}$$

where $K_p$ is proportional gain and $T_I$ is reset time.
The coefficients $K_p$ and $\frac{K_p}{T_I}$ are computed such that, at low frequency, the adjustable model stands alone, while at high frequency the reference model prevails.
The $\alpha$ and $\beta$ components of equation 3.14 are as in [16, 20]:

$$\frac{d\hat{\psi}_{s\alpha}}{dt} = \frac{1}{\sigma \tau_s} (-\hat{\psi}_{s\alpha} + k_r \hat{\psi}_{r\alpha}) + V_{s\alpha} - G(i_{s\alpha} - \hat{i}_{s\alpha}) \tag{3.16}$$

$$\frac{d\hat{\psi}_{s\beta}}{dt} = \frac{1}{\sigma \tau_s} (-\hat{\psi}_{s\beta} + k_r \hat{\psi}_{r\beta}) + V_{s\beta} - G(i_{s\beta} - \hat{i}_{s\beta}) \tag{3.17}$$

From equation 3.16 and 3.17, rotor flux expressed in terms of stator variables: as in [16]

$$\hat{\psi}_{r\alpha} = \frac{1}{k_r} \hat{\psi}_{s\alpha} - \frac{\sigma L_s}{k_r} i_{s\alpha} \tag{3.18}$$

$$\hat{\psi}_{r\beta} = \frac{1}{k_r} \hat{\psi}_{s\beta} - \frac{\sigma L_s}{k_r} i_{s\beta} \tag{3.19}$$

After both stator and rotor fluxes are estimated, it is possible to estimate the stator current as shown below.

$$\hat{i}_{s\alpha} = \frac{1}{\sigma L_s} \hat{\psi}_{s\alpha} - \frac{k_r}{\sigma L_s} \hat{\psi}_{r\alpha} \tag{3.20}$$

$$\hat{i}_{s\beta} = \frac{1}{\sigma L_s}\hat{\psi}_{s\beta} - \frac{k_r}{\sigma L_s}\hat{\psi}_{r\beta} \tag{3.21}$$

Figure 3.1 summarizes equations 3.16 to 3.21:

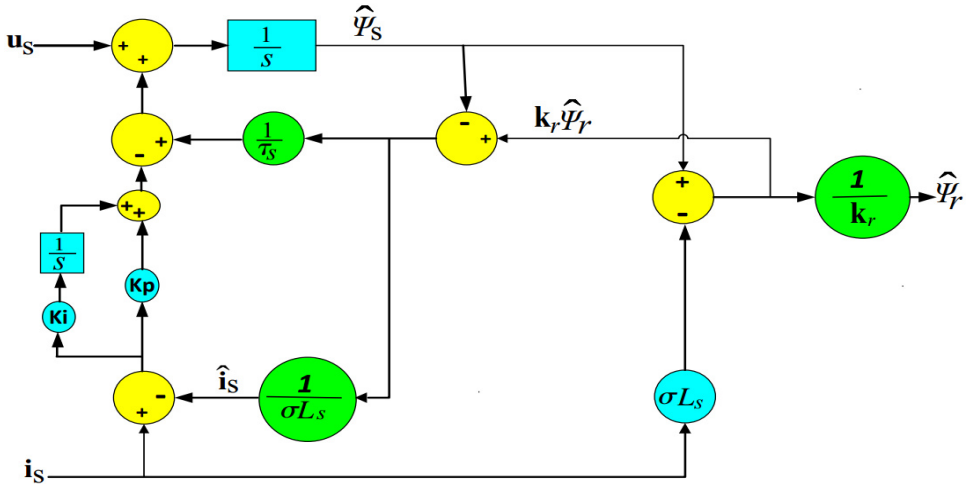


**Figure 3.1:** Luenberger observer(Flux estimator) updated from [1]

Figure 3.1 shows how LO observes rotor flux from measured phase current and voltage.

## 3.3 Observer gain selection

The Luenberger gain matrix is obtained by an expression that ensures the proportionality between the induction machines' eigenvalues and that of estimator's based on a G proportionality coefficient [10]. The observer gain G is chosen in such a way that, it imposes a fast dynamics for the observer [26]. As stated in [23] the gain G is designed to shift the observer poles to negative real values to ensure the stability of the observer system.
As stated in [38, 10, 26] observer gain could be expressed as::

$$G = \begin{bmatrix} g_1 I + g_2 J \\ g_3 I + g_4 J \end{bmatrix} = \begin{bmatrix} g_{11} & g_{12} & g_{21} & g_{22} \\ -g_{12} & g_{11} & -g_{22} & g_{21} \end{bmatrix}^T \tag{3.22}$$

Where: $\mathrm{I} = \begin{bmatrix} 1 & 0 \\ 0 & 1 \end{bmatrix}$ $J = \begin{bmatrix} 0 & -1 \\ 1 & 0 \end{bmatrix}$

The dynamic model of induction motor in stationary reference frame is given by:

$$\frac{d}{dt}\begin{bmatrix} I_{s\alpha} \\ I_{s\beta} \\ \psi_{r\alpha} \\ \psi_{r\beta} \end{bmatrix} = \begin{bmatrix} a_{11} & 0 & a_{13} & a_{14}\omega_r \\ 0 & a_{11} & -a_{14}\omega_r & a_{13} \\ a_{31} & 0 & a_{33} & a_{34} \\ 0 & a_{31} & -a_{34} & a_{33} \end{bmatrix} \begin{bmatrix} I_{s\alpha} \\ I_{s\beta} \\ \psi_{r\alpha} \\ \psi_{r\beta} \end{bmatrix} + \begin{bmatrix} \frac{U_{s\alpha}}{\sigma L_s} \\ \frac{U_{s\beta}}{\sigma L_s} \\ 0 \\ 0 \end{bmatrix} \tag{3.23}$$

where:
$a_{11} = a_{22} = -\left(\frac{R_s}{\sigma L_s} + \frac{{L_m}^2 R_r}{\sigma L_s {L_r}^2}\right), \quad a_{13} = a_{24} = \frac{R_r L_m}{\sigma L_s {L_r}^2}, \quad a_{14} = a_{23} = \frac{L_m}{\sigma L_s L_r}$
$a_{31} = a_{42} = \frac{R_r L_m}{L_r}, \quad a_{43} = a_{34} = \omega_{slp} = \omega_r, \quad a_{44} = a_{33} = -\frac{R_r}{L_r}$

Matrix A of equation 3.23 can be simplified to:

$$A = \begin{bmatrix} a_{11}I & a_{13}I + a_{14}J \\ a_{31}I & a_{33}I + a_{34}J \end{bmatrix} \tag{3.24}$$

The characteristic equation of the induction motor is given by:

$$|\lambda_{im} I - A| = 0 \tag{3.25}$$

Substituting values of equation 3.24 in to equation 3.25 and computing the determinant:

$$\begin{vmatrix} \lambda_{im} - a_{11}I & -(a_{13}I + a_{14}J) \\ -a_{31}I & \lambda_{im} - (a_{33}I + a_{34}J) \end{vmatrix} = 0 \tag{3.26}$$

$$(\lambda_{im} - a_{11}I)(\lambda_{im} - a_{33}I - a_{34}J) - a_{31}(a_{13}I + a_{14}J) = 0 \tag{3.27}$$

The characteristic equation of the observer is given by:

$$|\lambda_{lo} I - (A - GC)| = 0 \tag{3.28}$$

$$\begin{vmatrix} \lambda_{lo} - a_{11}I + G_1 I & -(a_{13}I + a_{14}J) \\ -a_{31}I + G_2 I & \lambda_{lo} - (a_{33}I + a_{34}J) \end{vmatrix} = 0 \tag{3.29}$$

$$(\lambda_{lo} - a_{11}I + G_1 I)(\lambda_{lo} - a_{33}I - a_{34}J) - (a_{31}I + G_2 I)(a_{13}I + a_{14}J) = 0 \tag{3.30}$$

As stated earlier the eigenvalues of the observer are proportional to those of the motor:

$$\lambda_{lo} = k * \lambda_{im} \tag{3.31}$$

Substituting equation 3.31 into equation 3.30 so that we can compare the result with equation 3.27.

$$(k\lambda_{im} - a_{11}I + G_1 I)(k\lambda_{im} - a_{33}I + a_{34}J) - (a_{31}I + G_2 I)(a_{13}I + a_{14}J) = 0 \tag{3.32}$$

Comparing equations 3.32 and equation 3.27 as in [27] results in the following equations.

$$g_{11} = (1-k)(a_{11} + a_{33}), \quad g_{12} = (1-k)\omega_r, \quad g_{21} = \left(1 - k^2\right)\left(a_{31} + \frac{a_{11}}{a_{14}}\right) - \frac{g_{11}}{a_{14}}, \quad g_{22} = \frac{g_{12}}{a_{14}}$$

k is a constant obtained by pole placement method. The larger the value of k, the faster the convergence of the observer will be, but if k is too large, the system would be very sensitive to noise signal, and results in reduced stability [28]. k is within a range of $[1-1.5]$ as given in [15] and k=1.3 is selected for the proposed observer.
Since the proposed observer estimates primarily only flux, it is enough to take only the rotor speed independent first term of the obtained Luenberger gain matrix [27].

## 3.4 Model Reference Adaptive System(MRAS)

Model reference adaptive system is effective speed estimation schemes over the other speed estimators such as extended Kalman filter (EKF), adaptive full order observer, reduced-order observer and Luenberger observer (LO) [3]. Nowadays, speed construction using proportional integral closed loop estimation schemes based on the model reference adaptive system was in interest particularly in the last decade, and it has been widely used for IM sensor-less speed control because of its relatively simple algorithm [28].

In adaptive system, in addition to the basic feedback structure, explicit measures are taken to automatically compensate for variations in the operating conditions, for variations in the process dynamics or for variations in the disturbances, in order to maintain an optimal performance of the system.

The reference model is a realization of the system with the desired performance. The basic philosophy behind Model Reference Adaptive Systems is to create a closed loop controller with parameters that can be adjusted based on the error between the output of the system and the desired response from the reference model. The control parameters converge to ideal values that cause the plant response to track the response of the reference model asymptotically with time for any bounded reference input signal [6].

**Rotor Flux Based MRAS Speed Estimator Design**

The rotor flux based MRAS speed estimator design is done with comparison between the estimated rotor flux of the voltage model (reference model) and estimated rotor flux of the current model (adaptive model) of the induction motor. A variety of MRAS schemes based on rotor flux, reactive power, active power, electromagnetic torque, fictitious quantity and back emf are available, but rotor flux based MRAS is the simplest approach to estimate the speed of AC machine drives [3]. Vector control by rotor flux orientation remains the most widely used as it offers high dynamic performance for a wide range of applications [18].

## 3.5 Stability Analysis

**Popov's Hyperstability Analysis**

As in [12] to insure the hyperstability of the given system, two conditions must be fulfilled. First, the linear time-invariant forward path transfer matrix $[SI-A]^{-1}$ must be strictly positive real and

second, the nonlinear feedback (which includes the adaptation mechanism) must satisfy Popov's criterion for stability. Popov's criterion for stability requires a finite negative limit on the input or output inner product of the nonlinear feedback system.

As in [37, 12]

$$\frac{d}{dt}\begin{bmatrix}\psi_{r\alpha}\\ \psi_{r\beta}\end{bmatrix} = \begin{bmatrix}-\frac{1}{\tau_r} & -\omega_r\\ \omega_r & -\frac{1}{\tau_r}\end{bmatrix}\begin{bmatrix}\psi_{r\alpha}\\ \psi_{r\beta}\end{bmatrix} + \frac{L_m}{\tau_r}\begin{bmatrix}i_{s\alpha}\\ i_{s\beta}\end{bmatrix} \tag{3.33}$$

$$\frac{d}{dt}\begin{bmatrix}\hat{\psi}_{r\alpha}\\ \hat{\psi}_{r\beta}\end{bmatrix} = \begin{bmatrix}-\frac{1}{\tau_r} & -\hat{\omega}_r\\ \hat{\omega}_r & -\frac{1}{\tau_r}\end{bmatrix}\begin{bmatrix}\hat{\psi}_{r\alpha}\\ \hat{\psi}_{r\beta}\end{bmatrix} + \frac{L_m}{\tau_r}\begin{bmatrix}i_{s\alpha}\\ i_{s\beta}\end{bmatrix} \tag{3.34}$$

Subtracting equations 3.33 from 3.34:

$$\frac{d}{dt}\begin{bmatrix}e_{\psi r\alpha}\\ e_{\psi r\beta}\end{bmatrix} = \begin{bmatrix}-\frac{1}{\tau} & -\omega_r\\ \omega_r & -\frac{1}{\tau}\end{bmatrix}\begin{bmatrix}e_{\psi r\alpha}\\ e_{\psi r\beta}\end{bmatrix} + \begin{bmatrix}0 & -e_{\omega r}\\ e_{\omega r} & 0\end{bmatrix}\begin{bmatrix}\hat{\psi}_{r\alpha}\\ \hat{\psi}_{r\beta}\end{bmatrix} \tag{3.35}$$

$$de_{\psi r} = Ae_{\psi r} - e_{\omega r}J\hat{\psi}_r \tag{3.36}$$

where: $e_{\psi r} = \begin{bmatrix}\hat{\psi}_{r\alpha} - \psi_{r\alpha} & \hat{\psi}_{r\beta} - \psi_{r\beta}\end{bmatrix}^T \quad e_{\omega r} = \hat{\omega}_r - \omega_r$

A core problem of model reference adaptive system is to identify its PI controller adaptation mechanism. As in [37] it is possible to define Popov's inequality as:

$$\forall t \geq 0, \quad \eta(0,t) = \int_0^t \Delta\psi^T(t)\Delta\omega(t)dt \geq -\gamma_0{}^2 \tag{3.37}$$

where $\gamma_0$ is a bounded positive constant.

Defining the symbols as follows:

$$\Delta\psi^T(t) = e_{\psi r} \quad \Delta\omega(t) = -e_{\omega r}J\psi \tag{3.38}$$

where: $J = \begin{bmatrix}0 & -1\\ 1 & 0\end{bmatrix} \quad \psi = \begin{bmatrix}\hat{\psi}_{r\alpha} & \hat{\psi}_{r\beta}\end{bmatrix}^T$

Substituting equations 3.38 into equation 3.37:

$$\eta(0,t) = -\int_0^t e_{\psi r}e_{\omega r}J\psi dt \geq -\gamma_0{}^2 \tag{3.39}$$

$$\eta(0,t) = \int_0^t \begin{bmatrix}\hat{\psi}_{r\alpha} - \psi_{r\alpha} & \hat{\psi}_{r\beta} - \psi_{r\beta}\end{bmatrix}^T(\omega_r - \hat{\omega}_r)\begin{bmatrix}0 & -1\\ 1 & 0\end{bmatrix}\begin{bmatrix}\hat{\psi}_{r\alpha} & \hat{\psi}_{r\beta}\end{bmatrix}^T dt \geq -\gamma_0{}^2$$

$$\eta(0,t) = \int_0^t (\hat{\omega}_r - \omega_r)(\psi^i{}_{r\beta}\hat{\psi}^i_{r\alpha} - \psi^i{}_{r\alpha}\hat{\psi}^i_{r\beta})dt \geq -\gamma_0{}^2 \tag{3.40}$$

$$\eta_1(0,t) = \int_0^t \hat{\omega}_r(\psi^i{}_{r\beta}\hat{\psi}^i_{r\alpha} - \psi^i{}_{r\alpha}\hat{\psi}^i_{r\beta})dt \geq -\gamma_1{}^2 \tag{3.41}$$

where:

$$\gamma_1{}^2 = \gamma_0{}^2 - \int_0^t \omega_r(\psi^i{}_{r\beta}\hat{\psi}^i_{r\alpha} - \psi^i{}_{r\alpha}\hat{\psi}^i_{r\beta})dt$$

The rotor flux equations of the reference model are :

$$\left\{\psi^i_{r\alpha} = \hat{\psi}^v_{r\alpha} \quad \psi^i_{r\beta} = \hat{\psi}^v_{r\beta}\right\}$$

Finally, the validity of the Popov's inequality of 3.41 can be verified provided that the adaptation mechanism of the rotor speed can be obtained by the following expression.

$$\hat{\omega}_r = k_i \int_0^t (\hat{\psi}^v_{r\beta}\hat{\psi}^i_{r\alpha} - \hat{\psi}^v_{r\alpha}\hat{\psi}^i_{r\beta})dt \tag{3.42}$$

As stated in [38, 27], to enhance the dynamic performance of the speed estimator the proportional term is added to equation 3.42. Then the speed adaptation mechanism becomes:

$$\hat{\omega}_r = k_p(\hat{\psi}^v_{r\beta}\hat{\psi}^i_{r\alpha} - \hat{\psi}^v_{r\alpha}\hat{\psi}^i_{r\beta}) + k_i \int_0^t (\hat{\psi}^v_{r\beta}\hat{\psi}^i_{r\alpha} - \hat{\psi}^v_{r\alpha}\hat{\psi}^i_{r\beta})dt \tag{3.43}$$

Then the error signal input to the PI controller is given by:

$$e_\omega = (\hat{\psi}^v_{r\beta}\hat{\psi}^i_{r\alpha} - \hat{\psi}^v_{r\alpha}\hat{\psi}^i_{r\beta})$$

### Lyapunov's Direct Method for Stability Analysis

The basic philosophy of Lyapunov's direct method is the mathematical extension of a fundamental physical observation: if the total energy of a system is continuously dissipated, then the system, whether linear or nonlinear, must eventually settle down to an equilibrium point. Thus, we may conclude the stability of a system by examining the variation of a single scalar function. This method can be summarized in the following three statements. For estimation error e, if

- V(e) is positive definite.
- $\frac{dV(e)}{dt}$ is negative definite.

Then the equilibrium at the origin is globally stable. Now applying the Lyapunov's stability analysis to guarantee the stability of the model reference adaptive controller over a wide range, it is possible to select a positive definite V as in [21] containing the state and speed error as shown in equation 3.44.

$$V = e^T e + \frac{(\hat{\omega}_r - \omega_r)^2}{\lambda} \tag{3.44}$$

where: $\lambda$ = positive constant
Assuming $\omega_r$ is constant and differentiating equation 3.44 with respect to time:

$$\frac{dV}{dt} = \dot{e}^T e + e^T \dot{e} + \frac{2}{\lambda}(\hat{\omega}_r - \omega_r)\frac{d\hat{\omega}_r}{dt} \tag{3.45}$$

$$\dot{x} = Ax + Bu \tag{3.46}$$

$$\dot{\hat{x}} = \hat{A}\hat{x} + Bu + G(Cx - C\hat{x}) \tag{3.47}$$

Taking the difference of equation 3.46 and 3.47

$$\dot{e} = (A + GC)e - \Delta A\hat{x} \tag{3.48}$$

Substituting equation 3.48 into equation 3.45

$$\frac{dV}{dt} = (e^T(A + GC)^T - \hat{x}^T\Delta A^T)e + e^T(A + GC)e - e^T\Delta A\hat{x} + \frac{2}{\lambda}(\hat{\omega}_r - \omega_r)\frac{d\hat{\omega}_r}{dt} \tag{3.49}$$

After some rearrangement:

$$\frac{dV}{dt} = e^T((A + GC) + (A + GC)^T)e - e^T\Delta A\hat{x} - \hat{x}^T\Delta A^T e + \frac{2}{\lambda}\Delta\omega_r\frac{d\hat{\omega}_r}{dt} \tag{3.50}$$

Selecting appropriate value of gain G so that the first term is negative definite and setting the remaining terms to zero:

$$-e^T\Delta A\hat{x} - \hat{x}^T\Delta A^T e + \frac{2}{\lambda}\Delta\omega_r\frac{d\hat{\omega}_r}{dt} = 0 \tag{3.51}$$

where:

$$\left\{\Delta A = \begin{bmatrix} 0 & \omega_r - \hat{\omega}_r \\ \hat{\omega}_r - \omega_r & 0 \end{bmatrix} \quad \hat{x} = \begin{bmatrix} \psi^i{}_{r\alpha} & \psi^i{}_{r\beta} \end{bmatrix}^T \quad e = \begin{bmatrix} \psi^v{}_{r\alpha} - \psi^i{}_{r\alpha} & \psi^v{}_{r\beta} - \psi^i{}_{r\beta} \end{bmatrix}^T\right\}$$

Substituting the above matrices into equation 3.51 and rearranging, results in:

$$\frac{d\hat{\omega}_r}{dt} = \frac{1}{\lambda}\left(\hat{\psi}^v_{r\beta}\hat{\psi}^i_{r\alpha} - \hat{\psi}^v_{r\alpha}\hat{\psi}^i_{r\beta}\right) \tag{3.52}$$

Or

$$\hat{\omega}_r = \frac{1}{\lambda}\int\left(\hat{\psi}^v_{r\beta}\hat{\psi}^i_{r\alpha} - \hat{\psi}^v_{r\alpha}\hat{\psi}^i_{r\beta}\right)dt \tag{3.53}$$

To enhance the dynamic performance of the speed estimator the proportional term is added.

$$\hat{\omega}_r = k_p\left(\hat{\psi}^v_{r\beta}\hat{\psi}^i_{r\alpha} - \hat{\psi}^v_{r\alpha}\hat{\psi}^i_{r\beta}\right) + k_i\int\left(\hat{\psi}^v_{r\beta}\hat{\psi}^i_{r\alpha} - \hat{\psi}^v_{r\alpha}\hat{\psi}^i_{r\beta}\right)dt \tag{3.54}$$

$k_p$ and $k_i$ are gains designed using Matlab /SISOTool, using the transfer function of the plant with designing constraints. The constraints considered are:
Percent of overshoot < 5%, Settling time < 2% seconds, Rise time < 2% seconds.
Using equation 3.34 and 3.54, it is possible to draw the following block-diagram.

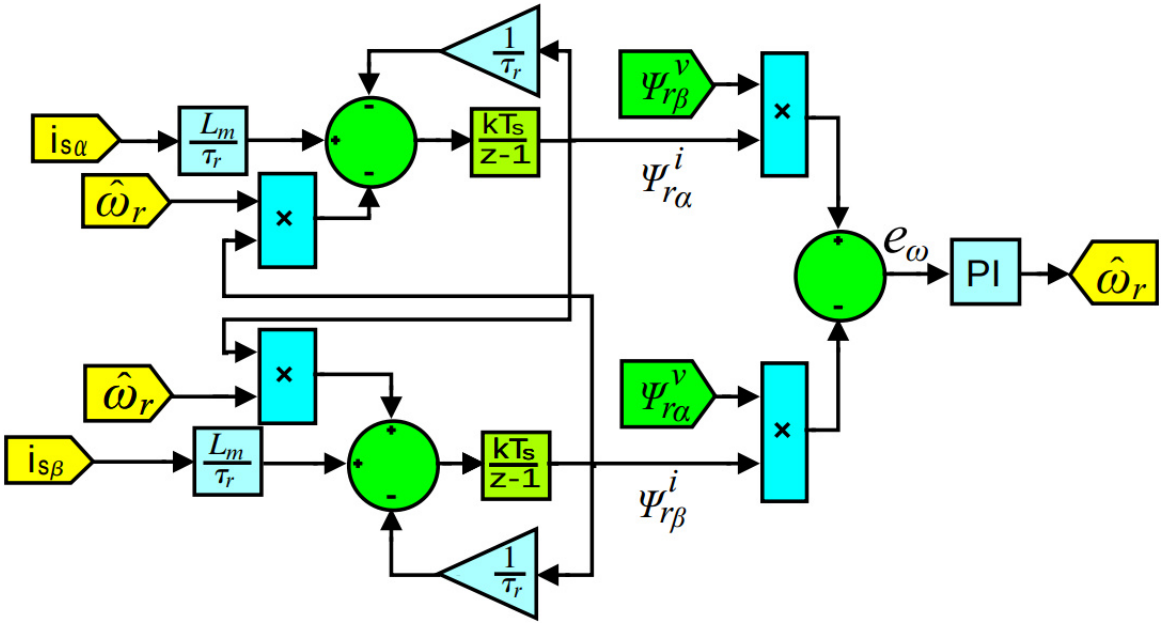


**Figure 3.2:** Adjustable model and adaptation mechanism system updated from [1]

The following block-diagram is obtained from equations 3.16 to 3.21, 3.34 and 3.54.

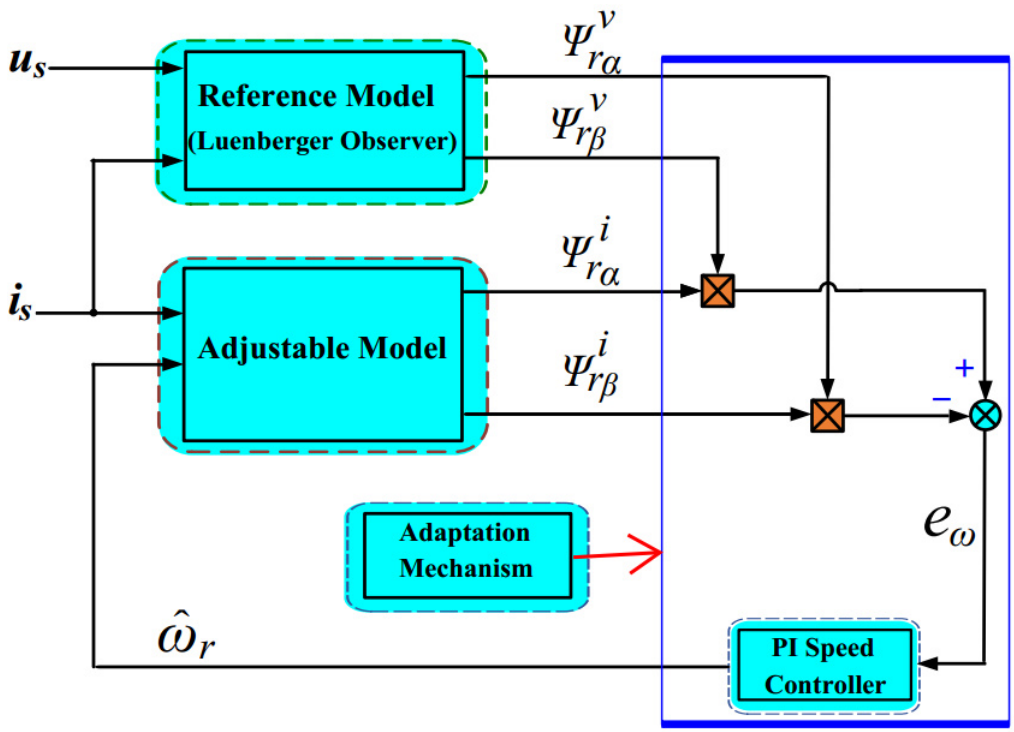


**Figure 3.3:** Model reference adaptive system updated from [37]

As shown in figure 3.2 and 3.3 both LO and the adjustable model require measured phase current, and the estimated speed is feedback to the adjustable model.

# 4 Simulation Results and Discussion

## 4.1 MATLAB/Simulink Modeling

Simulink is a well-known extension to MATLAB that allows engineers/users to rapidly and accurately build computer models of dynamical systems using block diagrams. It is capable of analyzing linear and nonlinear system models. That makes MATLAB/Simulink the best choice to use it for analyzing the proposed overall model. Analyzation of the system is started from modelling the overall block diagram, in such a way that each block diagram is modelled to represent its algorithms. Almost all block diagrams are available in the Simulink library, that is what makes MATLAB/Simulink one of the powerful engineering tool. After the block diagram is implemented in Simulink accurately, with appropriate ordinary differential equation and discrete or continuous time or both solver, depending on the nature of the model, behavior of the dynamic system can be analyzed.

## 4.2 Model of Associated MRAS and Luenberger Observer

A Simulink model of sensorless speed control of induction motor drive was developed by using existing components in simulink. The induction motor and the two- level inverter are used from the existing models. The direct Field Oriented Control (DFOC), space vector pulse width modulation(SVPWM) and the proposed flux observer and speed adaptation model is implemented using the theory outlined in Chapter two and three of this thesis and is shown in Figure 4.1. The induction motor used in this thesis is, a three phase squirrel cage type, with rated power of 180W and speed 1800rpm, parameters are given in Table 4.1.

**Table 4.1:** Parameters used for simulation

| | | | |
|---|---|---|---|
| Stator resistance | 1.7984Ω | $k_{i\omega}$ | 10 |
| Rotor Resistance | 1.588Ω | $K_{pId} = K_{pIq}$ | 200 |
| Stator Inductance | $0.3943H$ | $K_{iId} = K_{iIq}$ | 4 |
| rotor Inductance | $0.3947H$ | $K_{pmras}$ | 17800 |
| mutual Inductance | $0.387H$ | $K_{imras}$ | 4 |
| Moment of inertia | $0.0067kg.m^2$ | PWM Frequency | 5KHz |
| Viscous friction | 0.001N.m.s | $k_{p\psi}$ | 1980 |
| $k_{p\omega}$ | 18 | $k_{i\psi}$ | 1 |

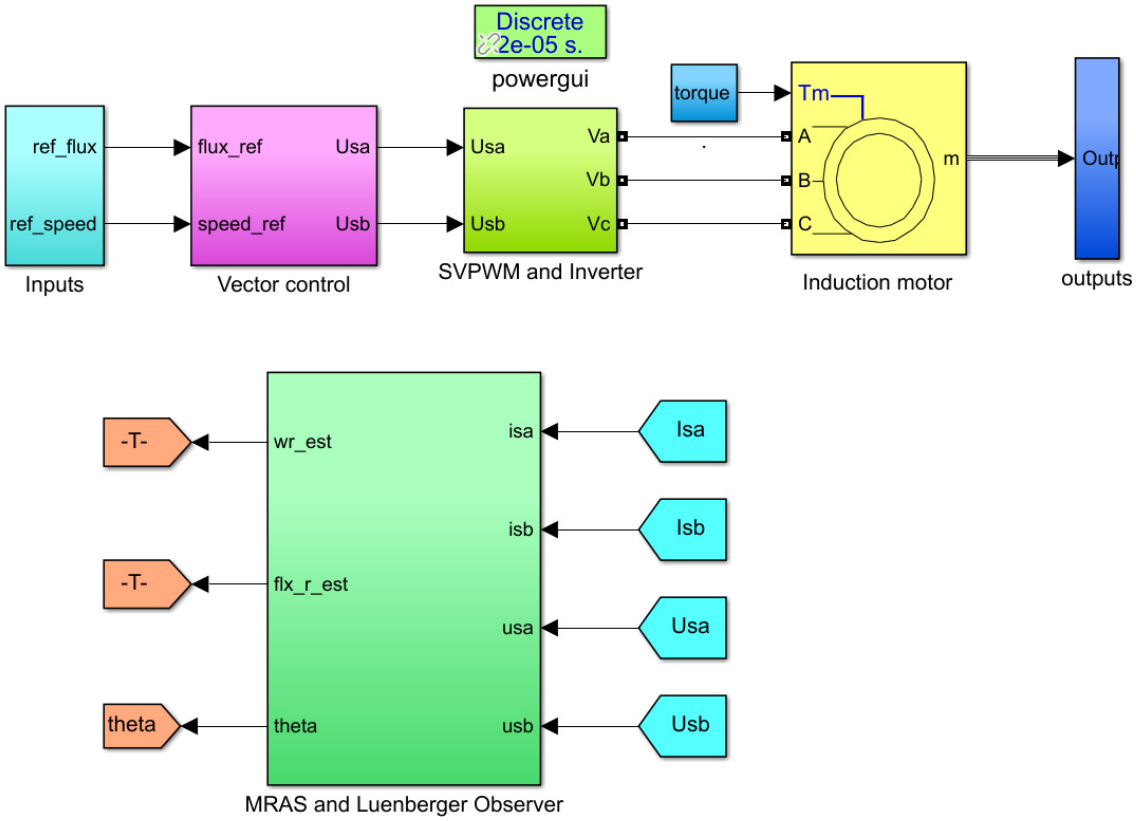


**Figure 4.1:** MRAS and Luenberger observer simulink model

The over all block diagram of the proposed controller indicated in figure 1.1 is implemented in matlab/simulink as shown in figure 4.1. At the very beginning rotor speed and rotor flux is placed, next the vector control part is shown, then after, SVPWM and inverter block is indicated where appropriate three phase input voltage and current is made ready. Next the induction motor is indicated. Finally, the observer part is implemented. Matlab Simulation of the proposed sensor-less speed control of induction motor drive was primarily carried out to measure the performance and robustness of the designed model. The performance of the designed model is highly dependent on the parameters of the IM to be controlled. So, the motor parameters should be well known.

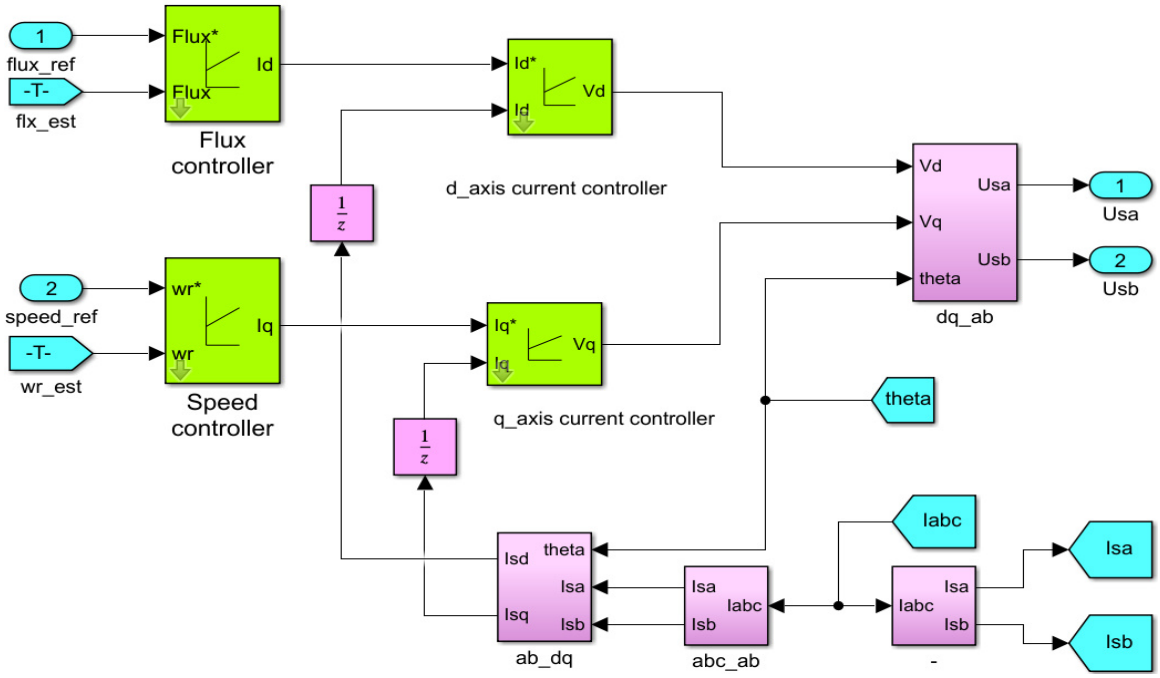


**(a)** Vector control

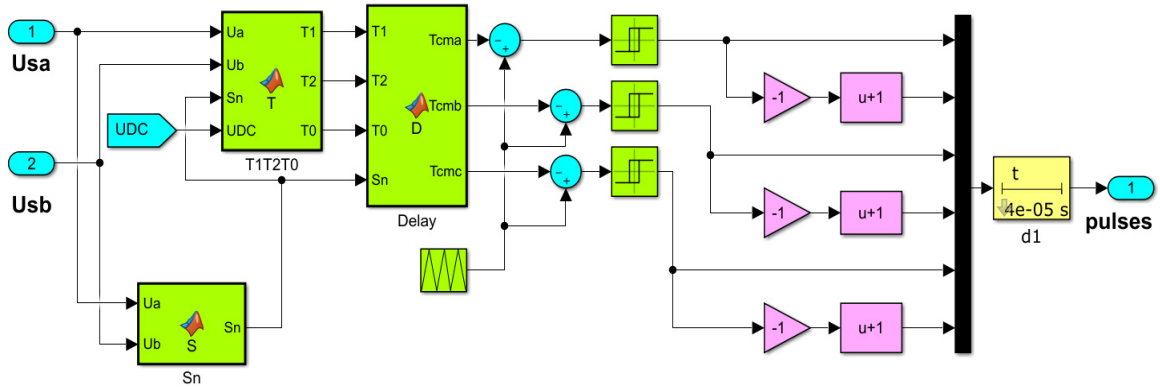


**(b)** Space vector pulse width modulation implementation

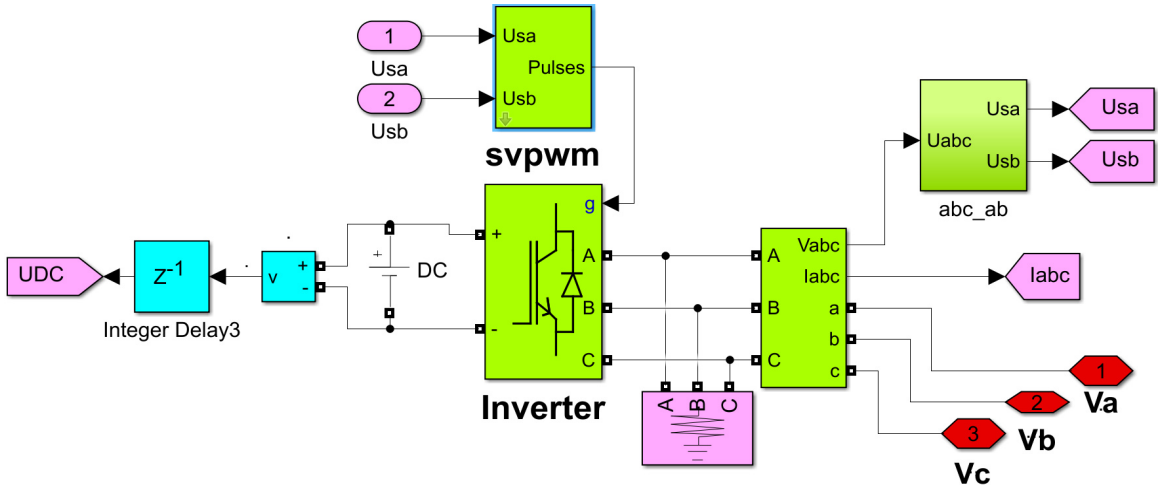


**(c)** Inverter, SVPWM & IM interconnection

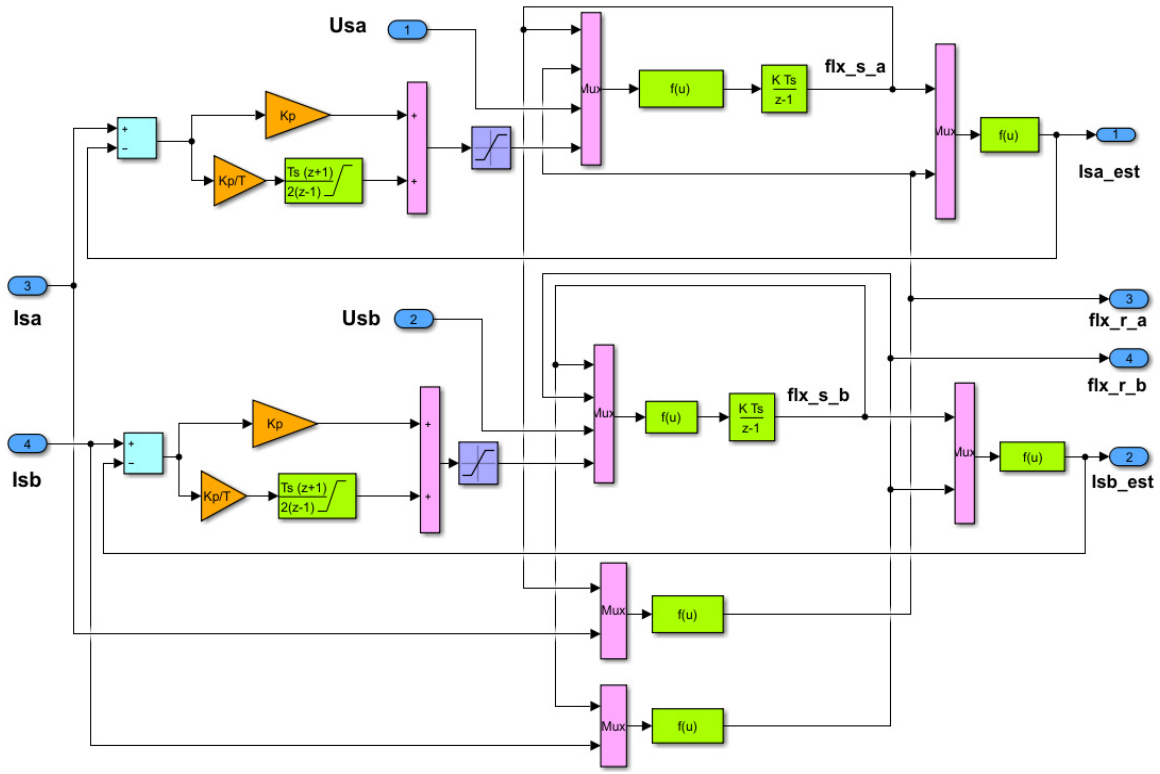


**(d)** Luenberger observer (Reference model)

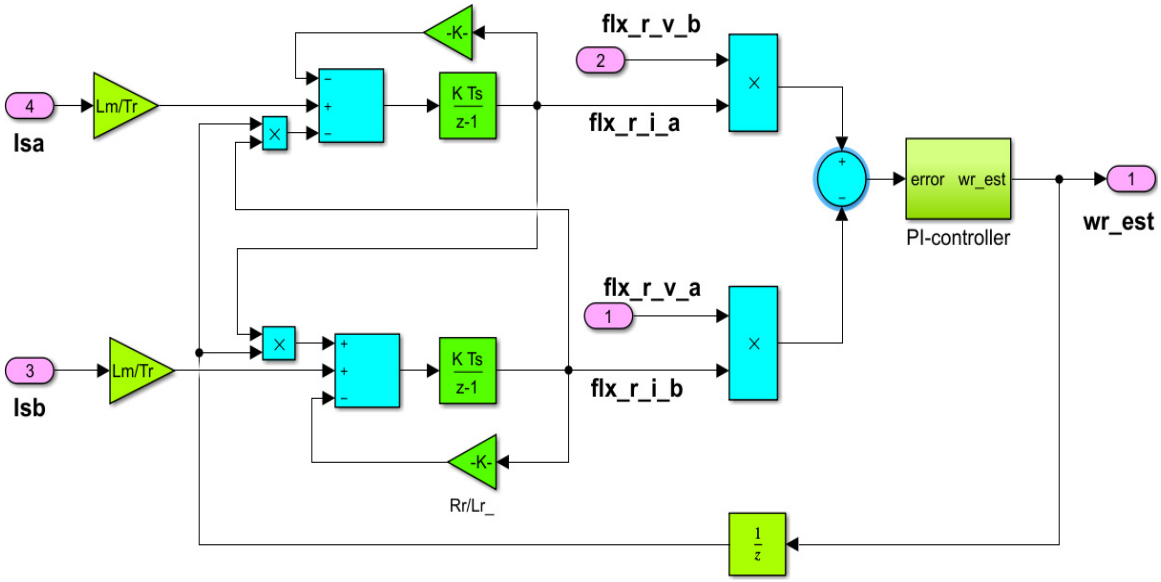


**(e)** Adjustable and adaptation mechanism model

**Figure 4.2:** Over all proposed system MATLAB implementation

The proposed MRAC and Luenberger Observer is used to analyze: Stator and rotor flux, Rotor speed, Torque response and sensitivity to motor parameter uncertainty.

## 4.3 Stator and Rotor Flux Analysis

For the Field oriented controller to work properly, the rotor flux must be estimated with a good accuracy. Because the park and clarke transformation are rotor flux position dependent. If the flux position is estimated wrongly, then everything fails.

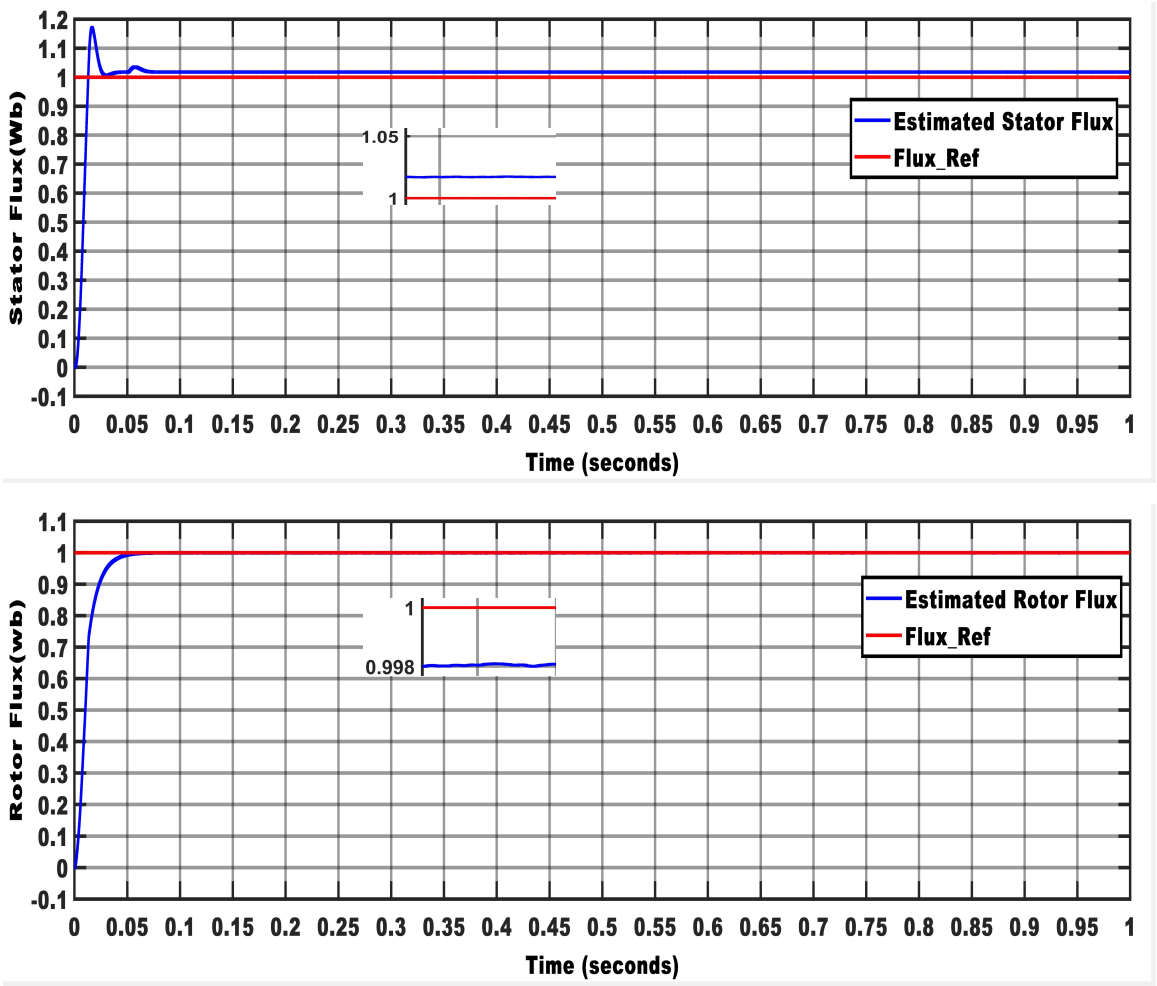


**Figure 4.3:** Estimated stator and Rotor Flux

Rotor flux is estimated with 0.024 seconds rise time, 0.2% steady state error and settling time of 0.05 seconds. Stator flux is estimated with 0.02 seconds rise time, 2% steady state error, settling time of 0.03 seconds and 17% of maximum overshoot.

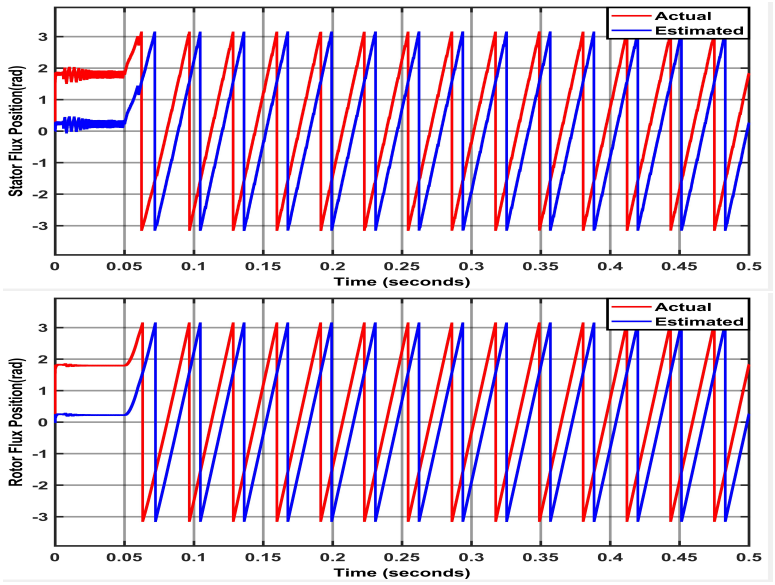


**Figure 4.4:** Estimated Stator and Flux Position (clockwise direction)

As shown in figures 4.3 the estimated stator flux has overshoot on the transient state due to high starting inrush current, but the estimated rotor flux does not have. Rotor flux position is estimated with a good accuracy, which is good input for the estimation of rotor speed. In figure 4.4 the stator and rotor flux position in motoring mode is estimated with a good accuracy except a slight phase difference.

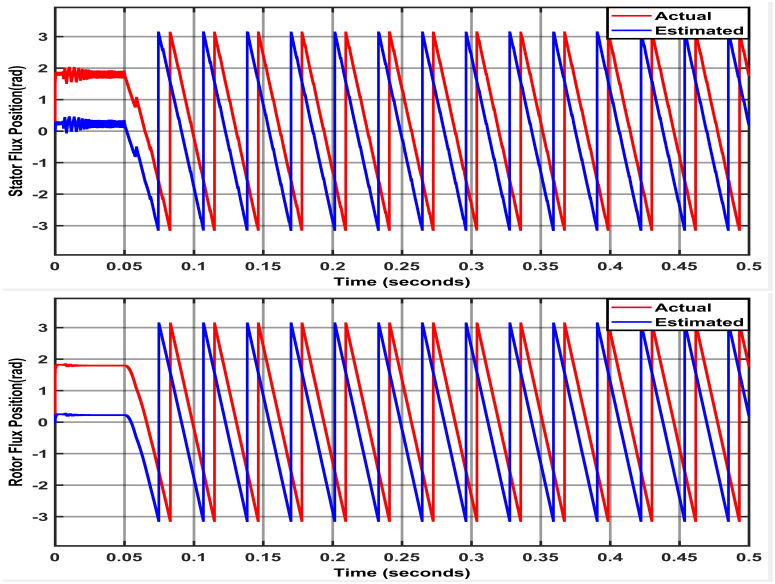


**Figure 4.5:** Estimated Stator and Rotor Flux Position (counter clockwise direction)

As shown in figure 4.5 stator and rotor flux position is estimated with a good accuracy except a slight phase difference in regenerative mode. So it is possible so proceed to the speed estimation part.

## 4.4 Speed response Analysis

Under this speed analysis part, the proposed MRAS and Luenberger observer based sensorless speed control of induction motor drive performance is tested in terms of:

- Different reference input tracking capability
- Low speed behavior
- Response of drive with speed reversal
- Torque response quickness
- Sensitivity to motor parameter variation

**Step input tracking capability**

Knowledge about the performance of an estimator, based on its ability of making the estimated speed to converge to the set point, especially during the transient period is crucial. This criterion is a well accepted as a primary indicator when measuring the performance of an estimator. It shows the converging ability of the estimated rotor speed to the actual one. The set point tracking capability of the proposed estimator can be analyzed by varying the speed reference of the system without altering the motor parameters.

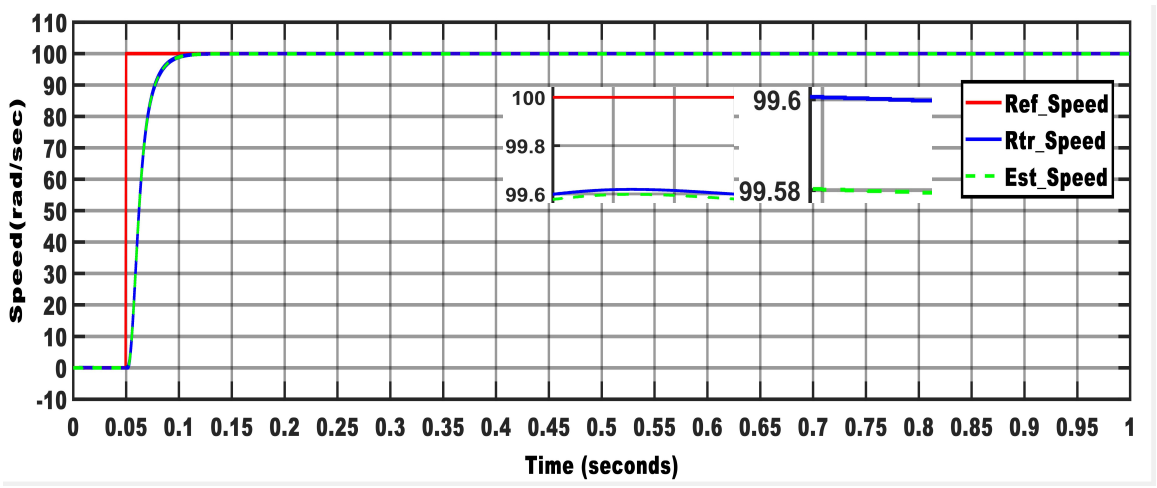


**Figure 4.6:** Speed response for step input

As shown in figure 4.6 the rotor speed is estimated with steady state error of 0.4%, rise time of 0.023 second, settling time of 0.05 second and the difference between rotor speed and estimated speed is 0.02rad/sec. This shows the good performance of the proposed estimator during transient and steady state.

**Different reference input speed tracking capability**

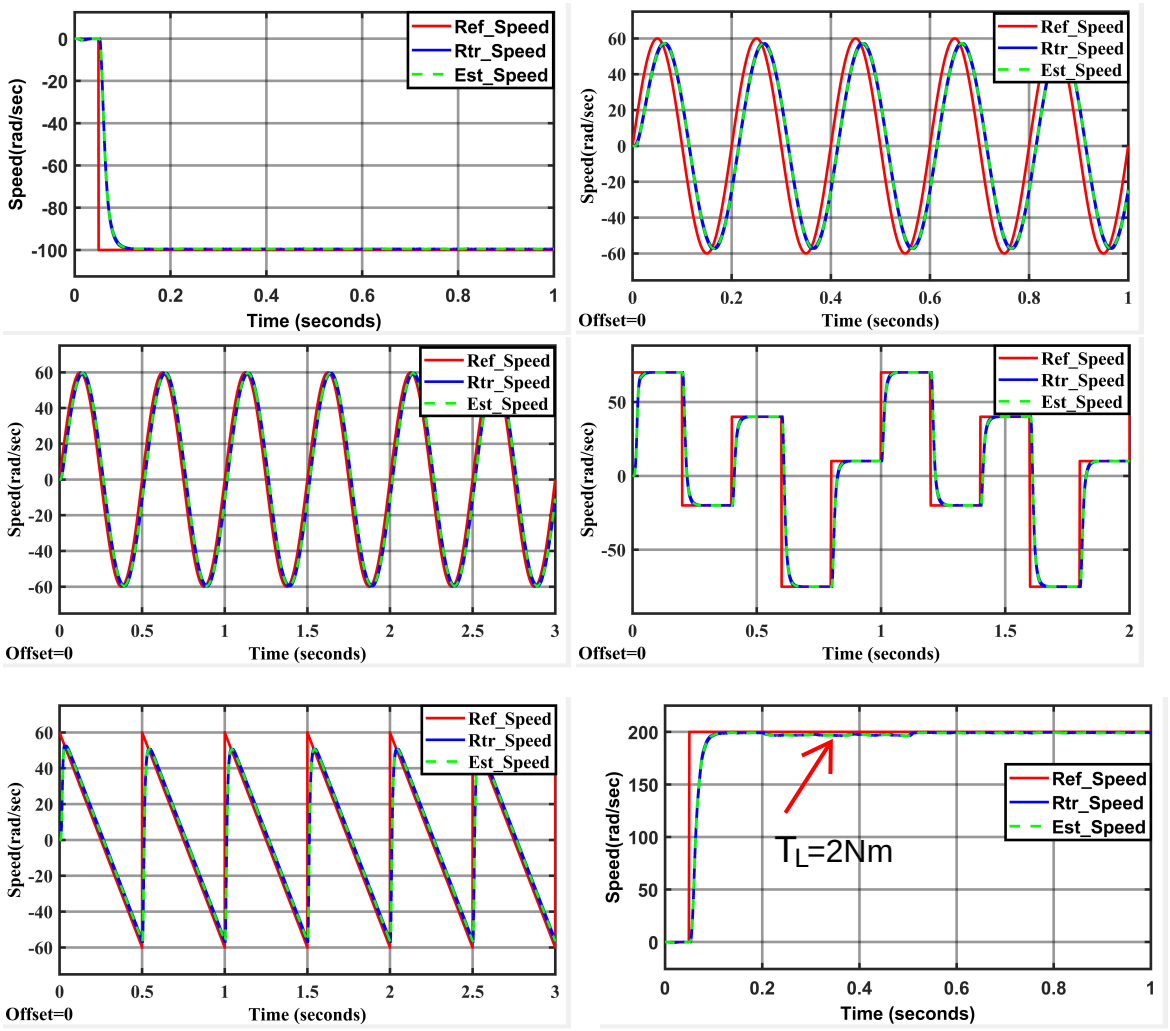


**(a)** Step input speed response with 2Nm Load Torque between 0.2-0.5sec

**Figure 4.7:** Speed response for different inputs

As shown in figure 4.7 the estimator tracks step, sinusoidal, and pulse inputs with a good accuracy. This implies the motor can work over a wide speed range. As frequency increase the observer can not reconstruct the states accurately, so the speed can not be tracked accurately as shown for the 2Hz and 5Hz sinusoidal inputs.

**Low speed behavior**

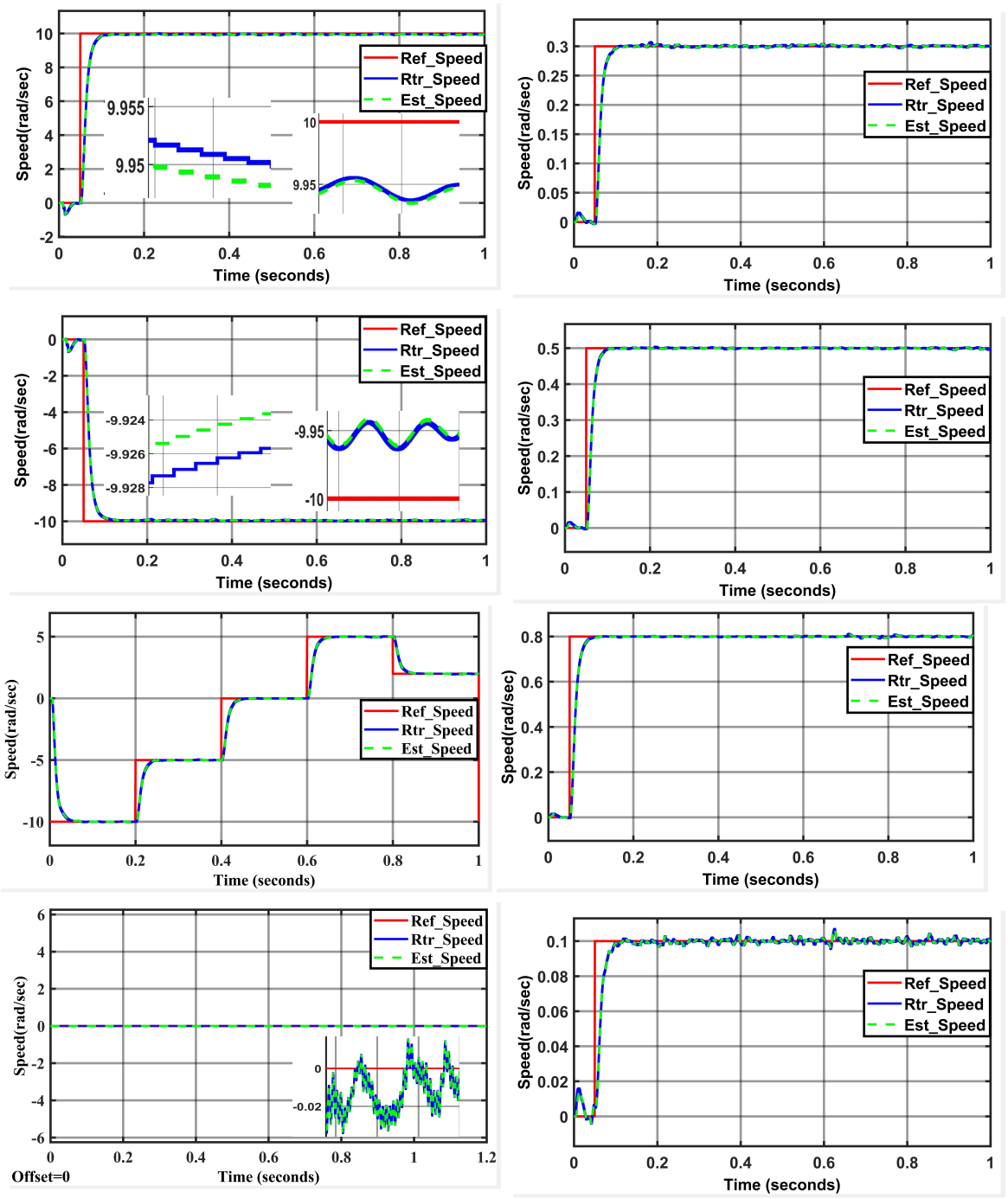


**Figure 4.8:** Low speed response for different inputs

Figure 4.8 illustrates the speed variation from -10 rad/sec to zero and zero to 10 rad/sec, speed response for variable step input ranging from -10 rad/sec to 5 rad/sec and zero speed response. The proposed model shows maximum of 0.022 rad/sec steady state error at zero speed, and 0.05rad/sec when running at 10 rad/sec and -10 rad/sec, and its low performance even at 0.3 rad/sec is great as error quickly converges to zero.

**Response of drive with speed reversal**

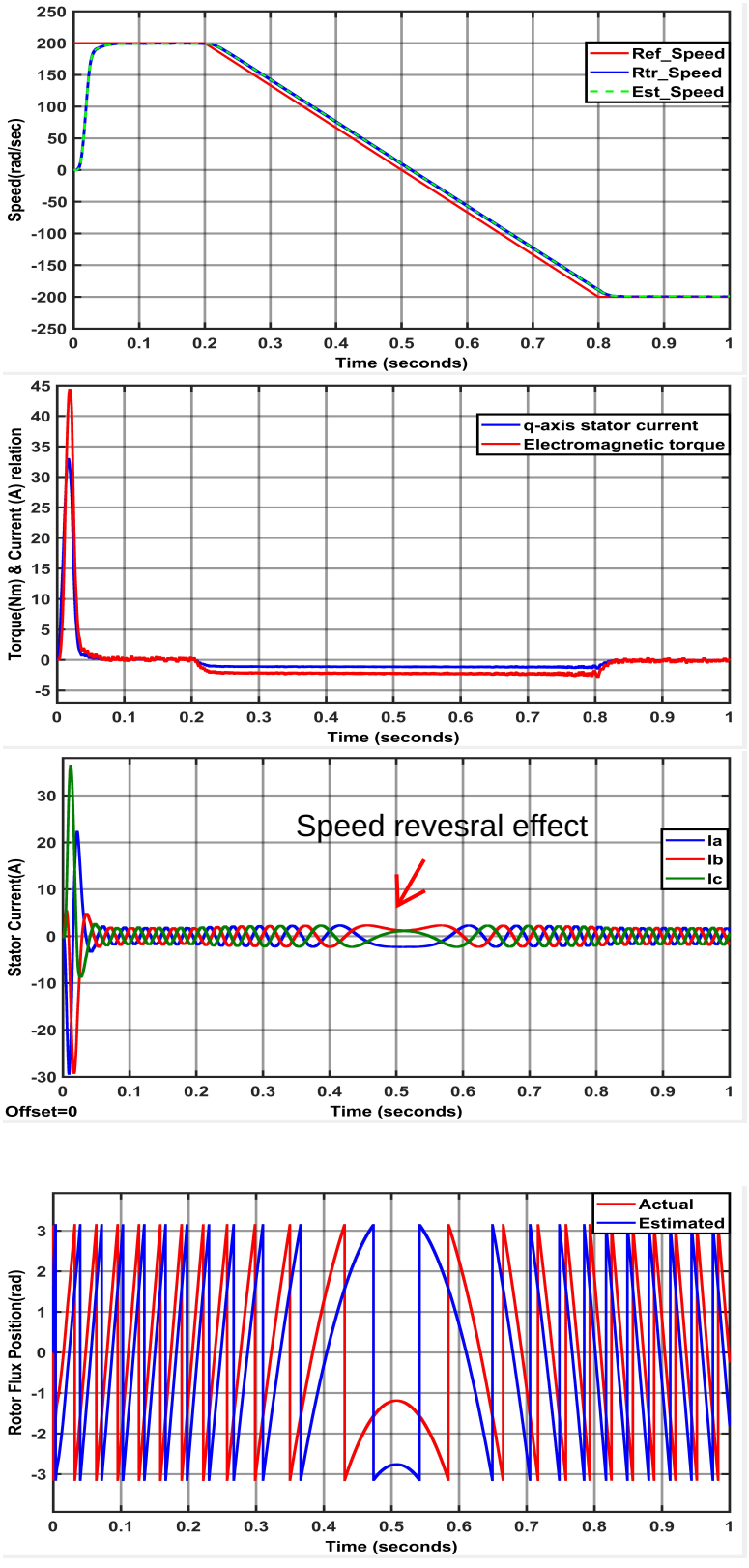


**Figure 4.9:** Torque, current, speed and flux position relationship

As shown in figure 4.9 ramp input speed signal decelerating over 0.2 - 0.8 second and constant between 0 - 0.2 second and 0.8 - 1.0 second. Since the input speed signal is decelerating over 0.2 - 0.8 second, the torque is negative over this interval, and is more negative than the q-axis stator current. The phase sequence of current is changed at 0.21 second approximately to change the direction of the speed of motor. The rotor and stator flux position flips.

## 4.5 Torque response analysis

As stated earlier the main goal of field oriented control is to decouple rotor flux and stator current, so that it is easier to control the electromagnetic torque using quadrature stator current alone keeping the direct axis rotor flux constant. In figure 4.9, 4.10 and 4.11, it is shown that the dynamic behavior of torque control is satisfactory and fully decoupled, enabling the fastest possible accelerations, deceleration, and reversing. So torque is directly controlled by the stator quadrature current.

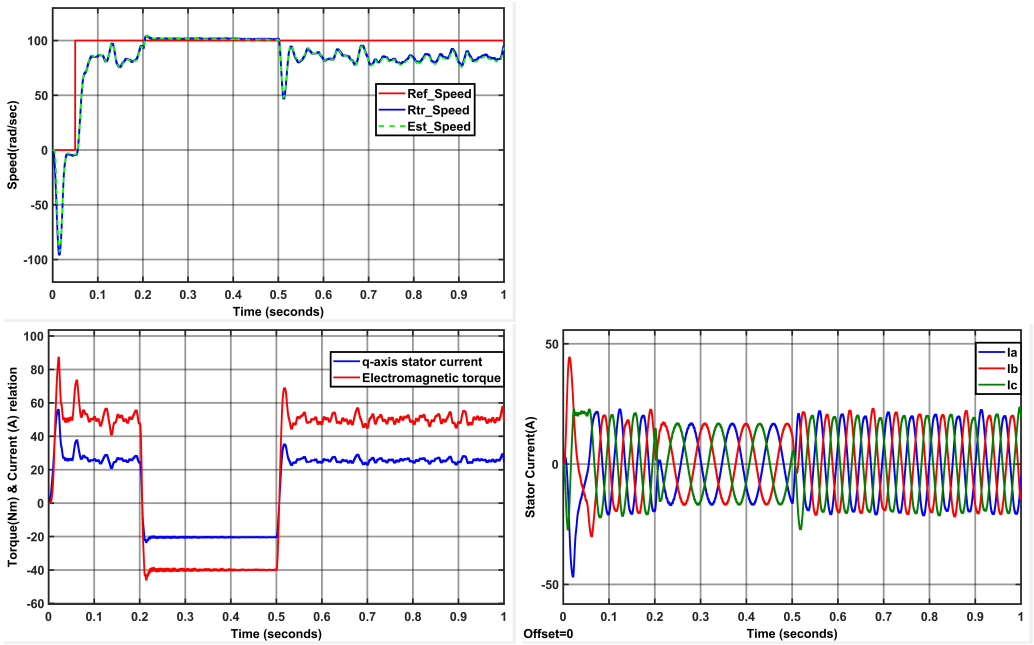


**Figure 4.10:** Torque, current and speed relationship

As shown in Figure 4.11, to test the torque response quickness 8Nm load torque is applied between 0.2 and 0.22 seconds as shown in the first figure , this results a drop in motor speed for a moment. This happens because of the mismatch in the torques, i.e. the developed torque is less than the load torque. To compensate for this mismatch, the controller increases the developed torque then the motor speed increases and gets back to the set point. In the second figure a 20Nm load torque is applied between 0.2 and 0.4 seconds, there is a reduction in speed between the indicated time intervals, although over rated load torque is applied the estimator does not release tracking.

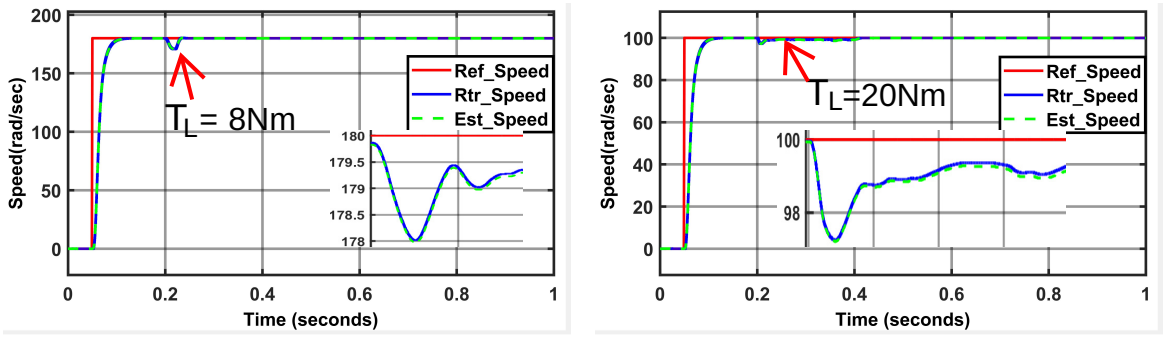


**Figure 4.11:** Torque effect on speed response

## 4.6 Sensitivity to motor parameter variation

It is well known that the estimator's robustness is highly induction motor parameters dependent, since the estimator model is directly extracted from the induction motor's dynamic equations. Induction motor parameters are altered by variations in temperature and saturation levels of the machine. Parameter variations tested in this thesis are the stator and rotor resistance. Among these parameters, stator resistance variation has large influence on the estimator's performance [13], supportive result in figure 4.12c and 4.12d. Rotor resistance has minimum effect but as the variation increases, the effect on the estimator's performance gets significant [13], supportive results are obtained and shown in figure 4.12a and 4.12b.

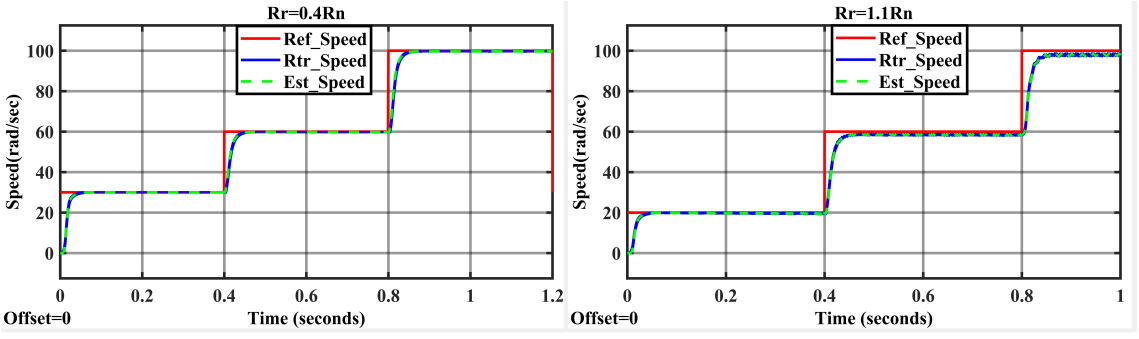


**(a)** 60% decrement in rotor resistance **(b)** 10% increment in rotor resistance

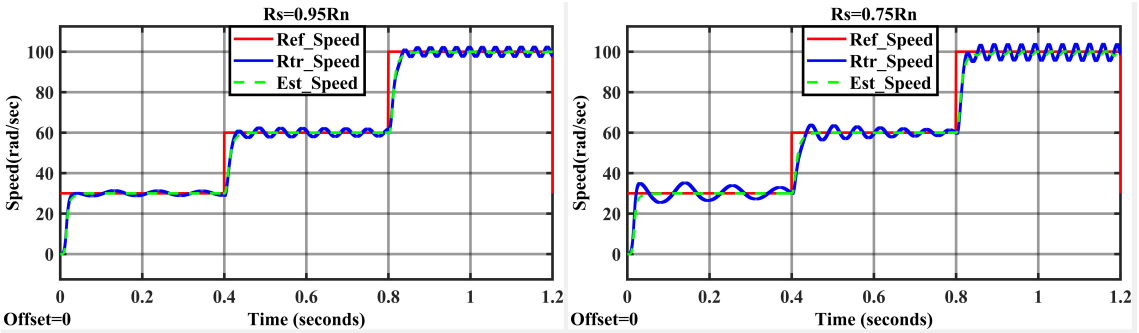


**(c)** 5% decrement in stator resistance **(d)** 25% decrement in stator resistance

**Figure 4.12:** Effect of rotor and stator resistance variation on tracking capability

# 5 Experimental Implementation

## 5.1 Introduction

The High Voltage Digital Motor Control (DMC) kit (HVMTRPFCKIT), is one of the crucial material to learn and experiment on digital control of high voltage motors. The kit contents and hardware details are discussed.

## 5.2 Kit Contents

The major parts of the kit are: F28035 controlCARD, High Voltage DMC board, 15V Power Supply, AC power Cord, Banana Plug Cords and USB-B to A Cable.

## 5.3 Features of HVMTRPFCKIT

The following are some of the features of the HVMTRPFCKIT kit [31]:
Three-Phase Inverter Stage to control high voltage motors, PFC stage rated for 750W, which can be used to increase the efficiency by shaping the input AC current and regulate the DC bus for the inverter to the desired level, Rectifier stage is rated up to 750W power and Auxiliary Power Supply Module (400V to15V & 5V module) which can generate 15V and 5V DC from rectified AC voltage or the PFC output (input Max voltage 400V).

## 5.4 Hardware Overview

The motor control board is divided into functional groups, so that the user can easily understand the complete motor drive system. The functional groups are named as macro blocks. List of the macro blocks and their functions are explained as follows:

- [*Main*] - ControlCARD connection, jumpers, communications (isoCAN), Instrumentation (DAC's), QEP and CAP connection and voltage translation.

- [$M1$] - AC power entry takes AC power from the wall/mains power supply and rectifies it. This can then be used for input of the PFC stage or used to generate the DC bus for the inverter directly.
- [$M2$] - Auxiliary power supply, 400V to 5V, and 15V module can generate 15V,5V power for the board from rectified AC power.
- [$M3$] - Isolated USB Emulation, provides isolated JTAG connection to the controller and can be used as isolated SCI when JTAG is not required.
- [$M4$] - Two-phase interleaved PFC stage can be used to increase efficiency of operation.
- [$M5$] - Three-phase inverter, to enable control of high voltage 3-phase motors.
- [$M6$] - DC power entry, generates 15V, 5V and 3.3V for the board from DC power fed through the DC-jack using the power supply shipped with the board.

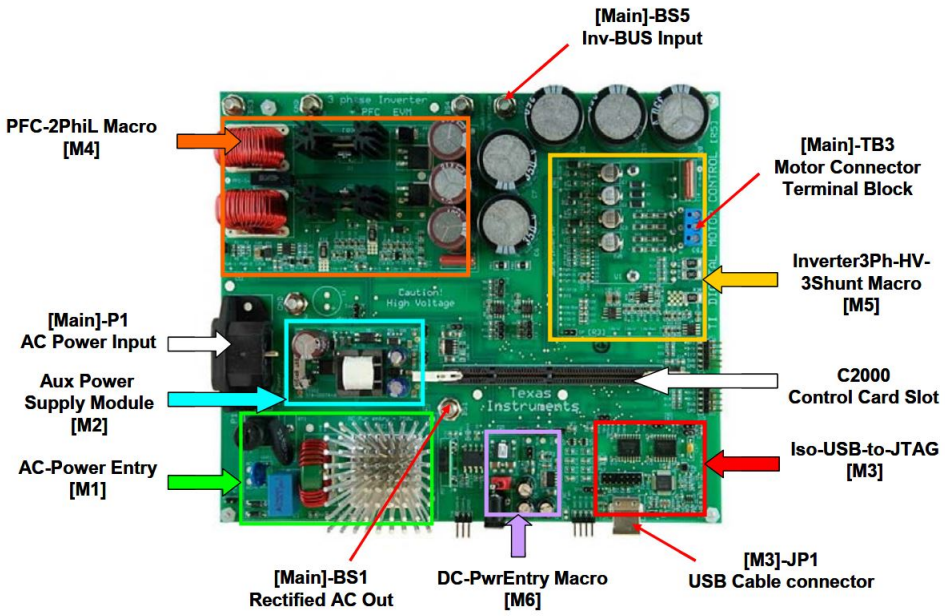


**Figure 5.1:** Inner view of HVMotorCtrlPFC Kit [31]

## 5.5 Powering the Board

The board contains two power domains

- The low voltage controller power domain that powers the micro-controller and the logic circuit present on the board.
- High voltage power delivery line that is used to carry the high voltage and current like the DC power for the Inverter also referred to as DC Bus.

## 5.6 Hardware Resource Mapping

Figure 5.2 shows the various stages of the board and illustrates the major connections and feedback values that are being mapped to the C2000 MCU.

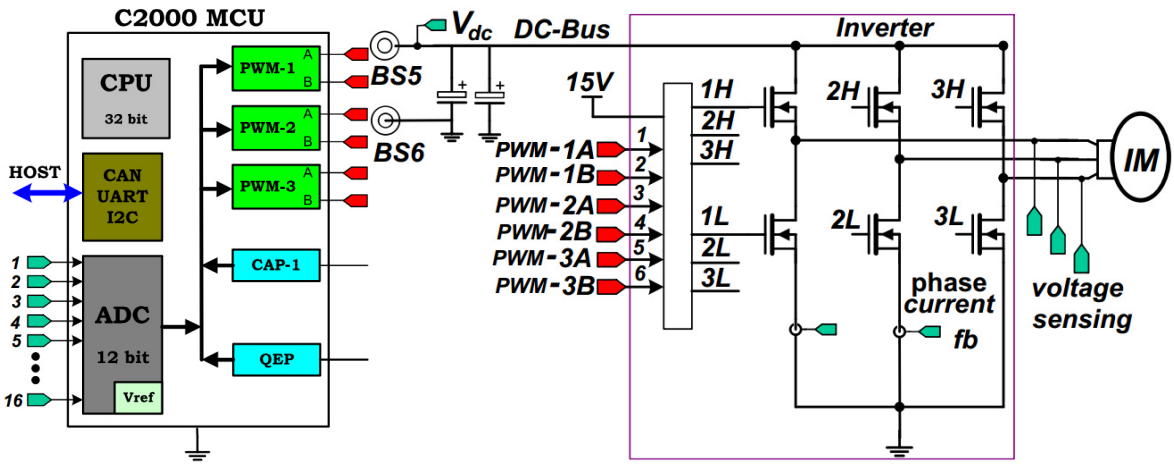


**(a)** C2000 MCU **(b)** High Voltage DMC

**Figure 5.2:** Three-phase Induction Motor Drive Implementation [2]

## 5.7 C2000 MCU

The C2000 controller family of devices perform the in need computation power to run complex control algorithms along with the right mix of peripherals to interface with the different components of the DMC (Digital motor control) hardware like, enhanced pulse width modulator (ePWM), analog to digital converter (ADC), enhanced Capture (ECAP), Quadrature Encoder Pulse (QEP), and so forth. The DMC Library provides configurable blocks that can be reused to implement new control strategies. IQMath Library enables easy migration from floating point algorithms to fixed point thus accelerating the development cycle. Therefore, with C2000 family of devices, it is easy and quick to implement complex control algorithms (sensored or sensorless) for motor control [2]. Some advantages of C2000 controllers:

- Favors system cost reduction by an efficient control in all speed range implying right dimensioning of power device circuits.
- Advanced control algorithms reduce harmonics generated by the inverter, reducing filter cost.
- Decreases the number of look-up tables that reduces the amount of memory required.

## 5.8 Development of Control Algorithm

The proposed system algorithm has initialization and interrupt subroutine module.

### Initialization module

Tasks performed by initialization module are DSP setup, variable initialization, interrupt source selection and enable and waiting loop which waits for indefinite time length until the interrupt sub

module sends the interrupt starting signal.

**Interrupt subroutine module description:**

The interrupt module is the main module where field oriented control algorithm is implemented. It updates stator voltage values in order to ensure the regulation of stator currents and rotor mechanical speed to their reference input value. Tasks performed by the Interrupt subroutine module are: Reading ADC output current value and scaling it up, Coordinate transformation, Rotor speed estimation ,Speed and current control and SVPWM algorithm.

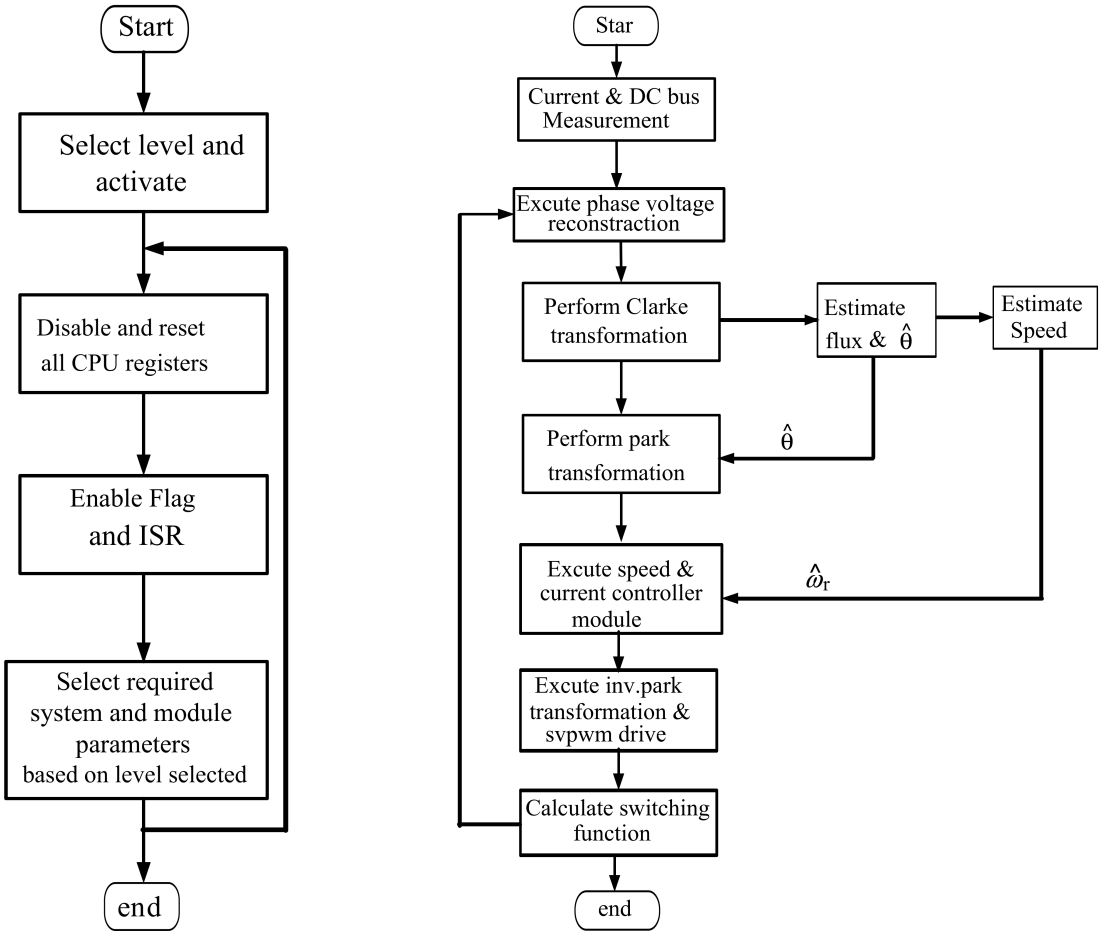


**Figure 5.3:** Flowchart of the proposed system

## 5.9 Experimental Setup

The experimental setup of the proposed sensor-less speed control of induction motor is shown in Figure 5.4.

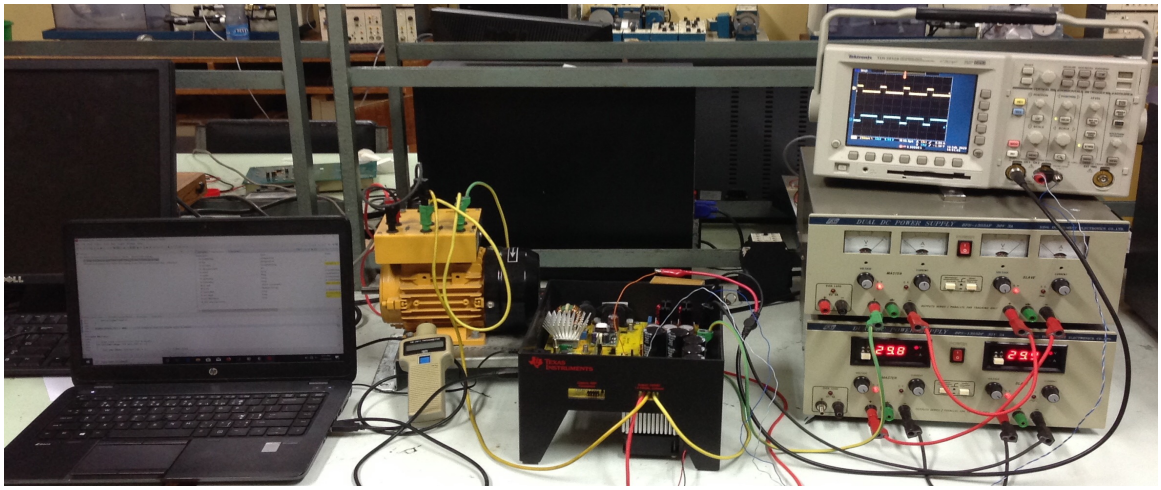

**Figure 5.4:** Experimental setup of the proposed system

The experimental setup consists of, any computer supporting code composer studio, to run the control algorithm, induction motor, the HVDMCMTRPFC kit connected to the computer by USB cable through the FTDI driver. The source code on the computer is debugged and loaded to the piccolo TMS320F28035 controller through the stated cable. The low voltage controller power domain generates 15V, 5V and 3.3V, that are used to power the controller card connected to the board, the logic, and sensing circuit assembled on the board. This power is obtained from Auxiliary Power supply module [M2]. DC bus power is high voltage line that feeds voltage for the inverter to generate three phase AC voltage to feed and control the motor. [Main]-BS5 and [Main]-BS6 are respectively the power and ground connector input of the inverter.

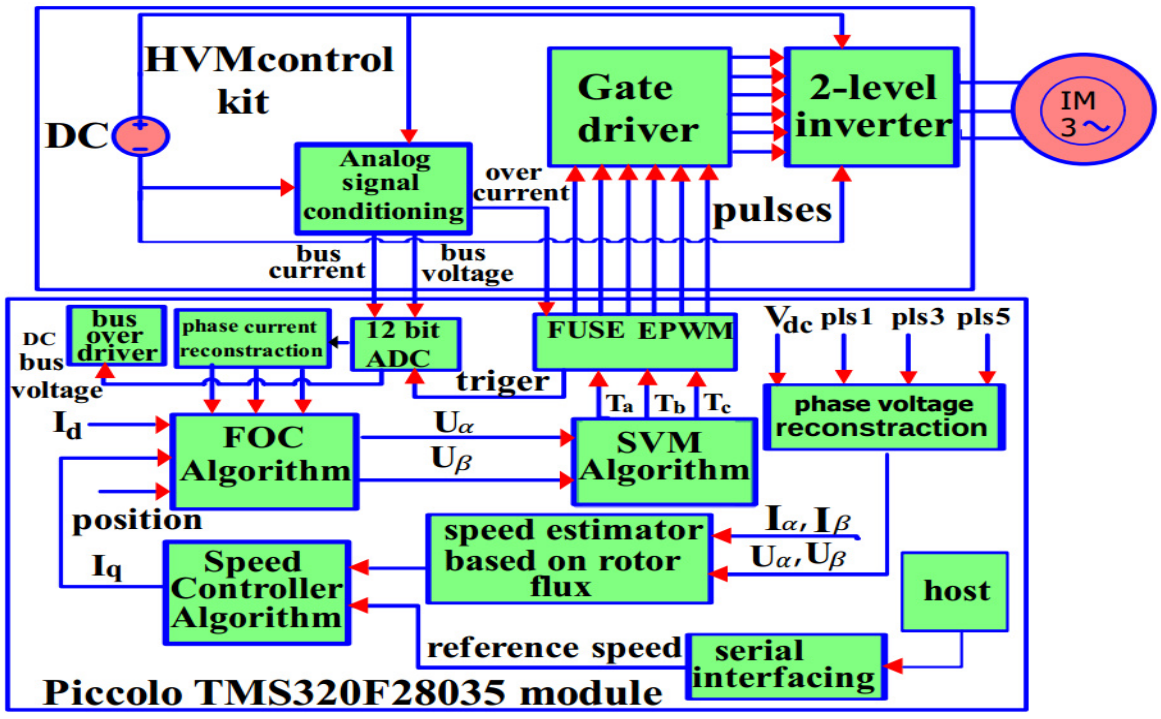


**Figure 5.5:** Experimental block diagram for speed control of IM updated from [31]

## 5.10 Experimental Results

The objective of this experimental demonstration is to control the motor speed using Pulse Width Modulation technique to generate appropriate sinusoidal voltage, that is used to feed the motor via the DSP kit, which is used to rotate the motor with any desired speed and direction. The rated speed is 1800rpm. The reference input speed is in pu.
The six control signals generated by the PWM are shown in Figure 5.6.

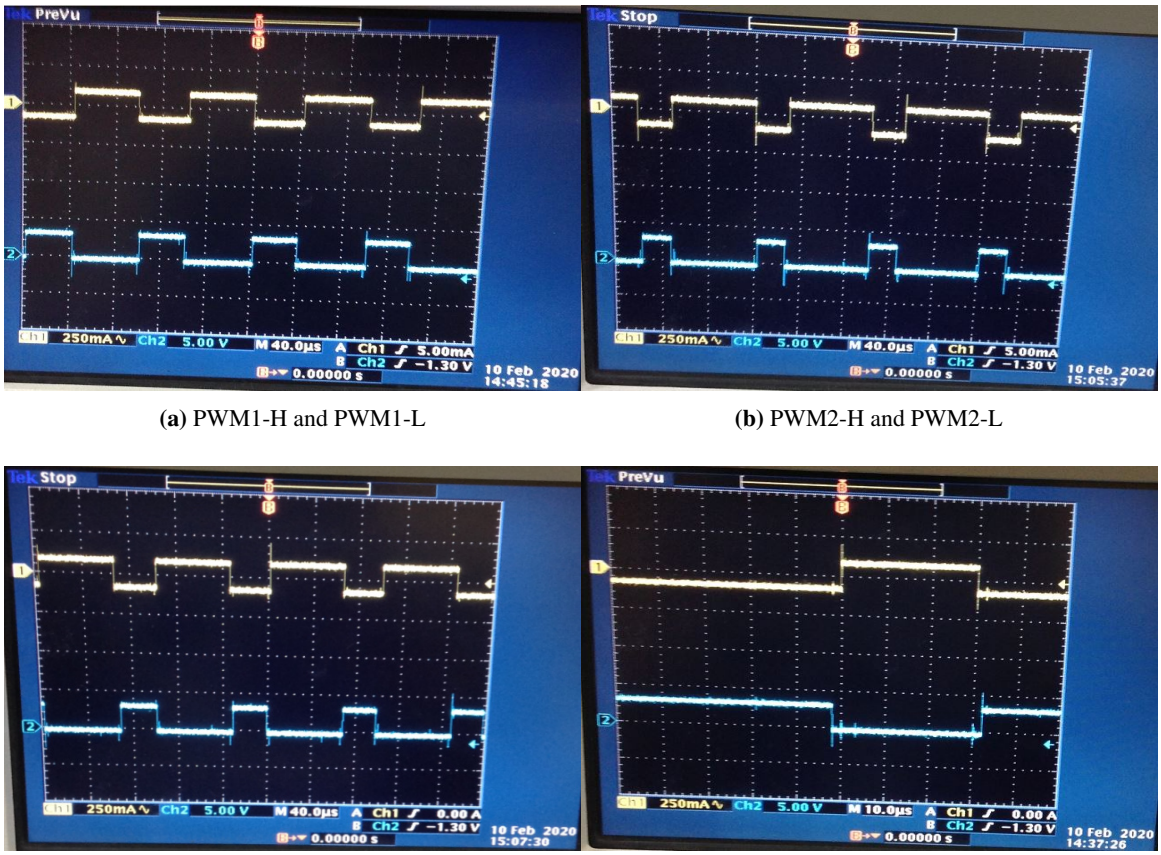


**(a)** PWM1-H and PWM1-L **(b)** PWM2-H and PWM2-L

**(c)** PWM3-H and PWM3-L **(d)** Angle difference between H and L

**Figure 5.6:** Modulated pulse signal taken from oscilloscope

Appropriate stator current and voltage generated by the control signal are given in figure 5.7a and 5.7b, which are used as input to the motor for a better operation of the estimator.

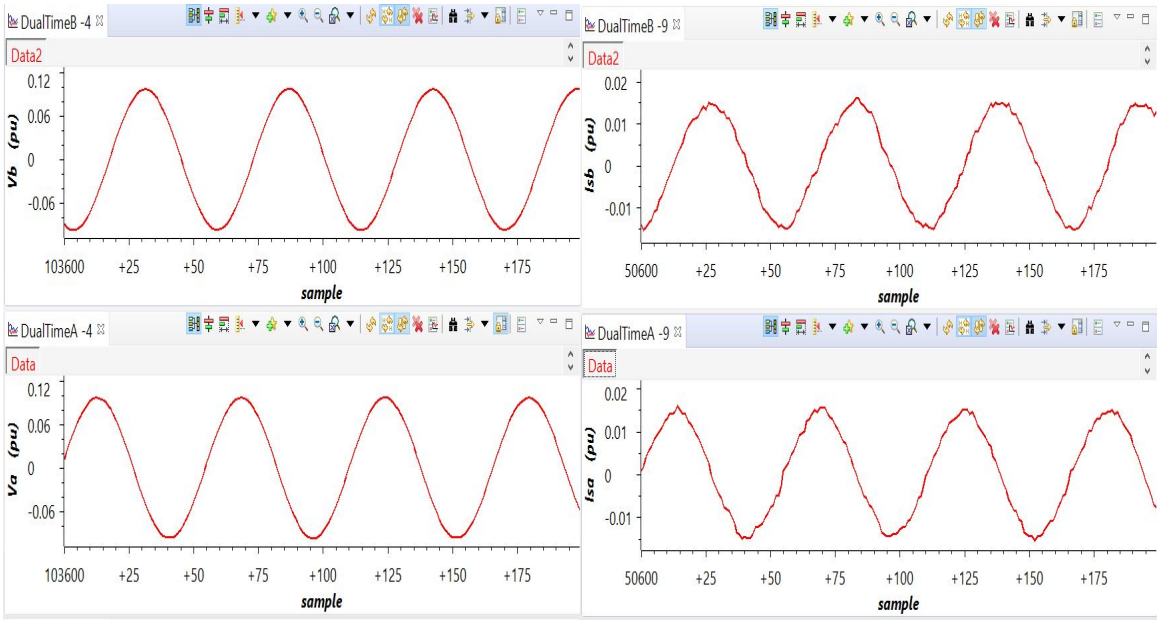


**(a)** Reconstructed stator phase voltage input to the IM **(b)** Stator phase current in stationary ref.frame

**Figure 5.7:** stator phase current and voltage taken from code composer studio

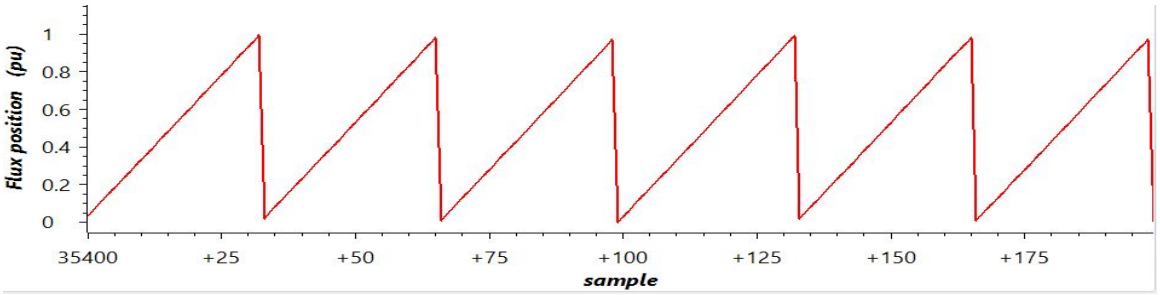


**(a)** Rotor flux position(clockwise)

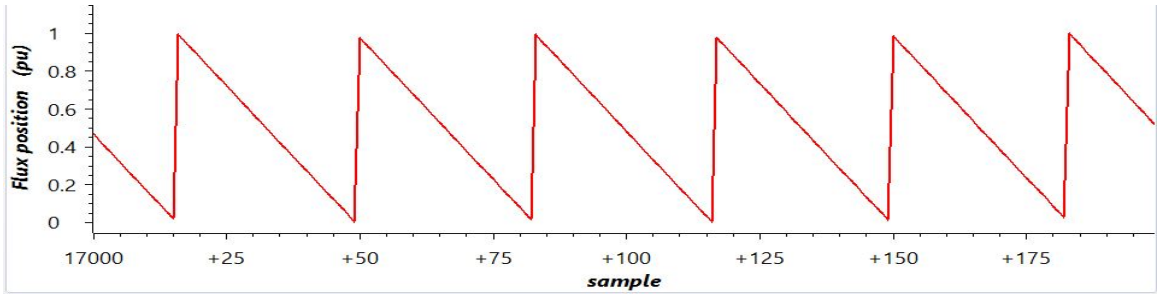


**(b)** Rotor flux position(counter clockwise)

**Figure 5.8:** Modulated pulse signal taken from code composer studio

Variables | Expressions | Registers

| Expression | Type | Value | Address |
|---|---|---|---|
| EnableFlag | unsigned int | 1 | 0x00009349@Data |
| Isw | unsigned int | 1 | 0x00009343@Data |
| IsrTicker | unsigned long | 22528652 | 0x0000936A@Data |
| dlog.prescalar | int | 5 | 0x0000944B@Data |
| IdRef | long | 0.09999996424 (Q-Value(24)) | 0x00009358@Data |
| IqRef | long | 0.04999995232 (Q-Value(24)) | 0x0000935A@Data |
| VdTesting | long | 0.1999999881 (Q-Value(24)) | 0x00009354@Data |
| VqTesting | long | 0.1999999881 (Q-Value(24)) | 0x00009356@Data |
| pi_spd | struct <unnamed> | {Ref=8388065,Fbk=8385024,... | 0x00009480@Data |
| CLA1 | Register Group | | |
| SpeedRef | long | 0.4999899864 (Q-Value(24)) | 0x0000935C@Data |
| se1.West | long | 0.4990897179 (Q-Value(24)) | 0x00009518@Data |
| se1.WestRpm | long | 1799 | 0x0000951C@Data |
| *Add new expression* | | | |

**(a)** Input,estimated and Actual rotor speed taken from code composer studio

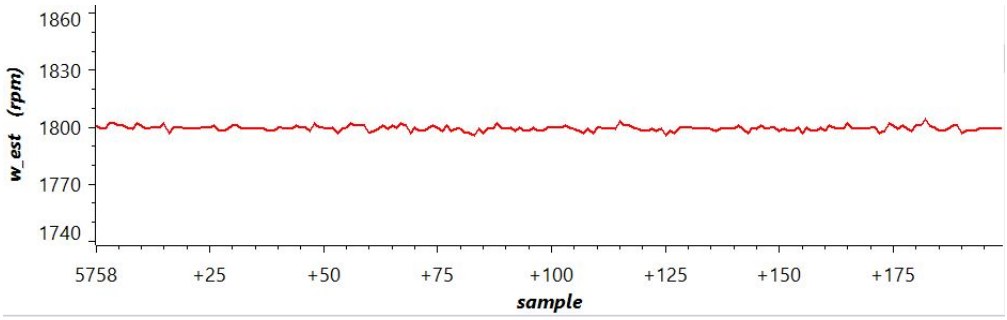


**(b)** Estimated rotor speed taken from code composer studio


**(c)** Actual rotor speed 1732rpm

**Figure 5.9:** Speed response for 1800rpm input

A shown in figure 5.9a steady state error of 3.2409666rpm is achieved.

Variables | Expressions | Registers

| Expression | Type | Value | Address |
|---|---|---|---|
| EnableFlag | unsigned int | 1 | 0x00009349@Data |
| lsw | unsigned int | 1 | 0x00009343@Data |
| IsrTicker | unsigned long | 54233452 | 0x0000936A@Data |
| dlog.prescalar | int | 5 | 0x0000944B@Data |
| IdRef | long | 0.09999996424 (Q-Value(24)) | 0x00009358@Data |
| IqRef | long | 0.04999995232 (Q-Value(24)) | 0x0000935A@Data |
| VdTesting | long | 0.1999999881 (Q-Value(24)) | 0x00009354@Data |
| VqTesting | long | 0.1999999881 (Q-Value(24)) | 0x00009356@Data |
| pi_spd | struct <unnamed> | {Ref=6710452,Fbk=6710112,... | 0x00009480@Data |
| CLA1 | Register Group | | |
| SpeedRef | long | 0.3999894261 (Q-Value(24)) | 0x0000935C@Data |
| se1.West | long | 0.3998875618 (Q-Value(24)) | 0x00009518@Data |
| se1.WestRpm | long | 1440 | 0x0000951C@Data |
| *Add new expression* | | | |

**(a)** Input,estimated and Actual rotor speed taken from code composer studio

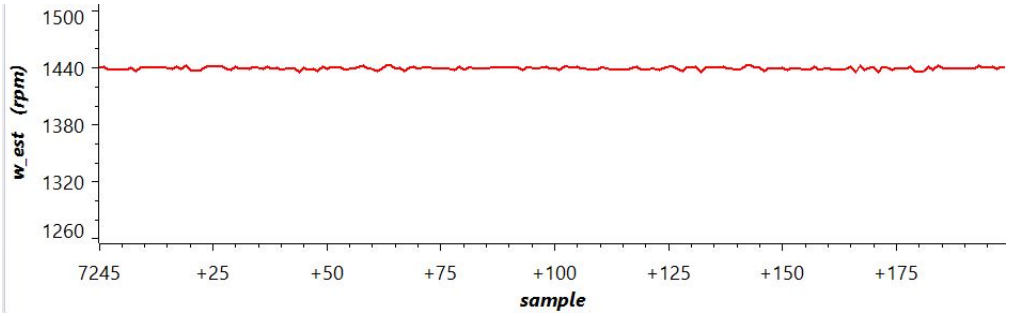


**(b)** Estimated rotor speed taken from code composer studio


**(c)** Actual rotor speed 1424.6rpm

**Figure 5.10:** Speed response for 1440rpm input

A shown in figure 5.10a steady state error of 0.36671148rpm is achieved.

Variables | Expressions | Registers

| Expression | Type | Value | Address |
|---|---|---|---|
| EnableFlag | unsigned int | 1 | 0x00009349@Data |
| Isw | unsigned int | 1 | 0x00009343@Data |
| IsrTicker | unsigned long | 27139886 | 0x0000936A@Data |
| dlog.prescalar | int | 5 | 0x0000944B@Data |
| IdRef | long | 0.09999996424 (Q-Value(24)) | 0x00009358@Data |
| IqRef | long | 0.04999995232 (Q-Value(24)) | 0x0000935A@Data |
| VdTesting | long | 0.1999999881 (Q-Value(24)) | 0x00009354@Data |
| VqTesting | long | 0.1999999881 (Q-Value(24)) | 0x00009356@Data |
| pi_spd | struct <unnamed> | {Ref=-5033350,Fbk=-5028880... | 0x00009480@Data |
| CLA1 | Register Group | | |
| SpeedRef | long | -0.2999898791 (Q-Value(24)) | 0x0000935C@Data |
| se1.West | long | -0.3000025749 (Q-Value(24)) | 0x00009518@Data |
| se1.WestRpm | long | -1081 | 0x0000951C@Data |
| *Add new expression* | | | |

**(a)** Input,estimated and Actual rotor speed taken from code composer studio

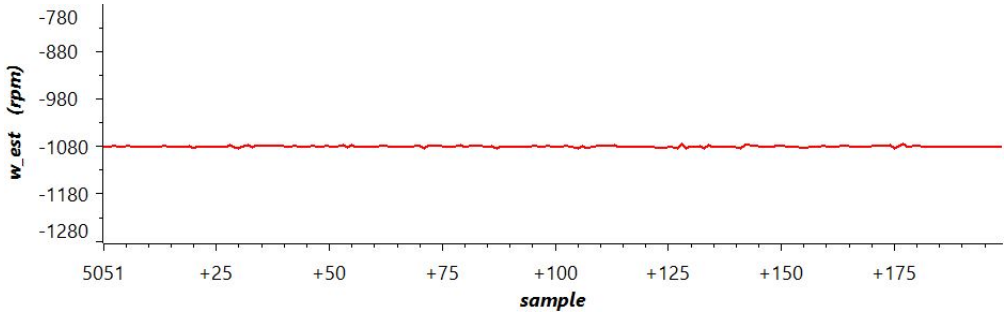


**(b)** Estimated rotor speed taken from code composer studio


**(c)** Actual rotor speed -1070.9rpm

**Figure 5.11:** Speed response for -1080rpm input

A shown in figure 5.11a steady state error of 0.04570488rpm is achieved.

Variables | Expressions | Registers

| Expression | Type | Value | Address |
|---|---|---|---|
| EnableFlag | unsigned int | 1 | 0x00009349@Data |
| Isw | unsigned int | 1 | 0x00009343@Data |
| IsrTicker | unsigned long | 35787207 | 0x0000936A@Data |
| dlog.prescalar | int | 5 | 0x0000944B@Data |
| IdRef | long | 0.09999996424 (Q-Value(24)) | 0x00009358@Data |
| IqRef | long | 0.04999995232 (Q-Value(24)) | 0x0000935A@Data |
| VdTesting | long | 0.1999999881 (Q-Value(24)) | 0x00009354@Data |
| VqTesting | long | 0.1999999881 (Q-Value(24)) | 0x00009356@Data |
| pi_spd | struct <unnamed> | {Ref=1677102,Fbk=1676808,... | 0x00009480@Data |
| CLA1 | Register Group | | |
| SpeedRef | long | 0.09998971224 (Q-Value(24)) | 0x0000935C@Data |
| se1.West | long | 0.0996799469 (Q-Value(24)) | 0x00009518@Data |
| se1.WestRpm | long | 358 | 0x0000951C@Data |
| *Add new expression* | | | |

**(a)** Input,estimated and Actual rotor speed taken from code composer studio

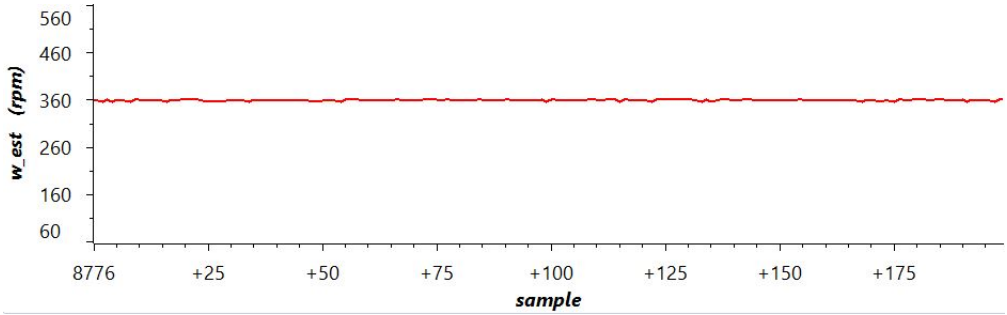


**(b)** Estimated rotor speed taken from code composer studio


**(c)** Actual rotor speed 360.8rpm

**Figure 5.12:** Speed response for 360rpm input

A shown in figure 5.12a steady state error of 1.115155224rpm is achieved.

# 6 Conclusion and Recommendation

## 6.1 Conclusion

In this thesis work, design and implementation of MRAS and Luenberger observer based speed estimator that can overcome the problems arising from mechanical speed sensor and motor parameter variation for speed control of induction motor has been investigated. The performance of the proposed MRAS and Luenberger observer was analyzed in terms of input tracking,torque response quickness, speed response at low speed and effect of parameter variation . It was observed that the estimator has good input speed tracking and torque response. The performance for parameter sensitivity showed that the MRAS and Luenberger observer response degrades as the uncertainty of the motor parameter variation increases. Input speed tracking ability of the proposed model is good. The system gives good performance at no load and loaded condition. Hence, it can work with different load torque conditions and with parameters variation. It was observed that among all parameters the stator resistance variation highly affect the observer performance. It was observed that stator resistance variation leads to instability of the MRAS and Luenbeger observer.

From the simulation results it is possible to deduce that MRAS and Luenberger observer based sensor-less speed controller of induction motor can estimate the rotor speed with a steady state estimation error of 0.4% and good transient response with rise time of 0.023 second and settling time of 0.05 second. Rotor flux is estimated with 0.024 second rise time, 0.2% steady state error and settling time of 0.05 second. Stator flux is estimated with 0.02 seconds rise time, 2% steady state error, settling time of 0.03 second and 17% of maximum overshoot.

It is shown that the dynamic performance, rotor flux and torque control are satisfactory and fully decoupled, enabling the fastest possible accelerations, decelerations, and reversing with the given torque limit.

Closed loop demonstration is carried out using Texas Instrument, Piccolo TMS320F28035 control card. With no load, maximum steady state error of 0.1800537% and good transient response has been achieved.

## 6.2 Recommendation

1. Due to the non linear characteristics of the induction motor,linear controller such as PI type controller fails to give optimum performance. So a better result can be obtained if sliding mode or fuzzy logic controller is used.this controller is also sensitive to parameter variation.

2. Above the rated speed , the controller can no longer maintain constant flux . So to control the motor speed above the rated speed Field weakening method is used. Therefore, operation of the proposed system can be extended to field weakening region.

# Bibliography


[1] H. Abu-Rub, A. Iqbal, and J. Guzinski. “HIGH PERFORMANCE CONTROL OF AC DRIVES WITH MATLAB/SIMULINK MODELS”. In: *John Wiley & Sons* (2012).

[2] B.Akin and M.Bhardwaj. “Sensorless Field Oriented Control of 3-Phase Induction Motors”. In: *Texas Instruments, Inc* (2013).

[3] A. Bhaumik and S. Das. “MRAS based Speed Sensorless Model Predictive Torque Control of Induction Motor Drive”. In: *IEEE Int. Conf. on Power Electron., Drives and Energy Syst. (PEDES)* (Dec. 2018).

[4] B.K. Bose. “Mordern power electronics and AC drives”. In: *Prentice Hall PTR* (2002).

[5] T. M. Chikouche et al. “Sensorless nonlinear control of a doubly fed induction motor using Luenberger observer”. In: *IEEE 4th Int. Conf. on Elect. Eng. (ICEE)* (Dec. 2015).

[6] N. D. Cuong. “Design of MRAS-based adaptive controllers for motion systems using linear motors”. In: *IEEE Int. Conf. on Inf. Sci., Electron. and Elect. Eng.* (Apr. 2014).

[7] Turan Gonen. “Electrical Machines with MATLAB®”. In: *Crc press* Second Ed. (2012).

[8] Osvaldo González et al. “Speed sensorless predictive current control of a five-phase induction machine”. In: *2017 12th IEEE Conference on Industrial Electronics and Applications (ICIEA)*. 2017, pp. 343–348.

[9] J. Guzinski, H.Abu-Rub, and P. Strankowski. “Variable Speed ac drives with inverter Output Filters”. In: *John Wiley and Sons* (2015).

[10] H.Chalawane, A. Essadki, and T. Nasser. “MRAS and Luenberger observers using a SIFLC controller in adaptive mechanism based sensorless fuzzy logic control of induction motor”. In: *IEEE Int. Conf. on Elect. and Inf. Technol. (ICEIT)* (May 2016).

[11] V. T. Ha et al. “Sensorless speed control of a three-phase induction motor: An experiment approach”. In: *IEEE Int. Conf. on Syst. Sci. and Eng. (ICSSE)* (July 2017).

[12] H. He and J. Xing. “Design of Induction Motor Speed-Sensorless Vector Control System”. In: *IEEE Int. Symp. on Comput., Consum. and Control (IS3C)* (July 2016).

[13] A. Iqbal and M. A. Husain. “MRAS based Sensorless Control of Induction Motor based on Rotor Flux”. In: *IEEE Int. Conf. on Comput. and Characterization Techn. in Eng. & Sci. (CCTES)* (Sept. 2018).

[14] R. Kamaleshwar, A. Prahadeeshwaran, and N. SrivatsAthindran. “Sensorless sliding mode control of SVPWM fed induction motor drive using dss speed estimator”. In: *IEEE Int. Conf. on Innov. Res. In Elect. Sci. (IICIRES)* (June 2017).

[15] P. Karlovsky and J. Lettl. “Improvement of DTC performance using luenberger observer for flux estimation”. In: *IEEE 18th Int. Sci. Conf. on Elect. Power Eng. (EPE)* (May 2017).

[16] M. R. Khan and A. Iqbal. “Model reference adaptive system with simple sensorless flux observer for induction motor drive”. In: *IEEE Int. Conf. on Power Electron., Drives and Energy Syst. (PEDES)* (Dec. 2012).

[17] T.S. Kwon, M.H. Shin, and D.S. Hyun. “Speed Sensorless Stator Flux-Oriented Control of Induction Motor in the Field Weakening Region Using Luenberger Observer”. In: *IEEE Trans. on Power Electron.* 20.4 (July 2005), pp. 864–869.

[18] Y. Laatra, H. Lotfi, and B. Abdelhani. “Speed sensorless vector control of induction machine with Luenberger observer and Kalman filter”. In: *IEEE 4th Int. Conf. on Control, Decision and Inf. Technol. (CoDIT)* (Apr. 2017).

[19] Y.S. Lai and Y.T. Chang. “Design and implementation of vector-controlled induction motor drives using random switching technique with constant sampling frequency”. In: *IEEE Trans. on Power Electron.* 16.3 (May 2001), pp. 400–409.

[20] P. Liu and L. Hao. “Vector Control-Based Speed Sensorless Control of Induction Motors using Sliding-Mode Controller”. In: *IEEE 6th World Congr. on Intell. Control and Automat.* (2006).

[21] Y.C. Luo, Y.H.Chen, and W.C.Pu. “Sensorless Air-Gap Flux Vector Control Induction Motor Drive Based on Particle Swarm Optimization Algorithm Flux Observer”. In: *IEEE Int. Symp. on Comput., Consum. and Control (IS3C)* (Dec. 2018).

[22] M. Morey and V. Virulkar. “Rotor Flux Observer for Speed Sensorless IFOC Induction Motor at Low Speeds”. In: *IEEE Int. Conf. on Power Electron., Drives and Energy Syst. PEDES* (Dec. 2018).

[23] K. Pavel and L. Jiri. “Influence of speed and flux estimation by Luenberger observer on IM drive with DTC”. In: *IEEE Int. Conf. on Appl. Electron. (AE)* (Sept. 2017).

[24] Satish Kumar Peddapelli. *Pulse width modulation: analysis and performance in multilevel inverters*. Walter de Gruyter GmbH & Co KG, 2016.

[25] Chao-Chung Peng. “Nonlinear Integral Type Observer Design for State Estimation and Unknown Input Reconstruction”. In: *Applied Sciences* 7.1 (2017), p. 67.

[26] S.Belkacem et al. “Speed sensorless DTC of induction motor based on an improved adaptive flux observer”. In: *IEEE Int. Conf. on Ind. Technol.* (Jan. 2006), pp. 1192–1197.

[27] S.Saha and B. Nayak. “Sensorless vector control and selection of observer gain for speed control of indirect vector control induction motor drives”. In: *IEEE 2nd Int. Conf. on Elect.,Comput. and Commun. Technol. (ICECCT)* (Feb. 2017).

[28] L. Shi et al. “Speed sensorless vector control oflnduction motor based on adaptive full-order flux observer”. In: *IEEE 11th Conf. on Ind. Electron. and Appl. (ICIEA)* (June 2016).

[29] M.Pasko T.Białoń A. Lewicki and R.Niestrój. “Non-proportional full-order Luenberger observers of induction motors”. In: *Archives of Electrical Engineering* 67 (Jan. 2018), pp. 925–937.

[30] M.Pasko T.Białoń A. Lewicki and R.Niestrój. “PI observer stability and application in an induction motor control system”. In: *Bulletin of the Polish Academy of Sciences. Technical Sciences* 61.3 (2013), pp. 595–598.

[31] Workagegn Tatek. *Model Reference Adaptive Control Based Sensorless Speed Control of Induction Motor*. Addis Ababa Institute of Technology, 2017.

[32] Hamid A Toliyat and Steven G Campbell. *DSP-based electromechanical motion control*. CRC press, 2003.

[33] V.Tiwari, S.Das, and A.Pal. “Sensorless speed control of induction motor drive using extended kalman filter observer”. In: (2017), pp. 1–6.

[34] P. Vas. “Sensorless vector and direct torque control”. In: *Oxford Univ. Press* (1998).

[35] BT Venu Gopal. “Comparison Between Direct and Indirect Field Oriented Control of Induction Motor”. In: *Int. J. of Eng. Trends and Technol. (IJETT)* 43.6 (2017), pp. 364–369.

[36] H. H. Vo et al. “Fuzzy model-based speed observer for sensorless induction motor drive with PWM-DTC”. In: *IEEE ELEKTRO* (May 2018).

[37] H. Wang, X. Ge, and Y.C. Liu. “Second-Order Sliding-Mode MRAS Observer-Based Sensorless Vector Control of Linear Induction Motor Drives for Medium-Low Speed Maglev Applications”. In: *IEEE Trans. on Ind. Electron.* 65.12 (Dec. 2018), pp. 9938–9952.

[38] Y.Cui et al. “Adaptive Full-Order Observer for Induction Motor Based on Bilinear Transformation Method”. In: *IEEE 21st Int. Conf. on Elect. Mach. and Syst. (ICEMS)* (Oct. 2018).

[39] Y.Zhang et al. “A comparative study of Luenberger observer, sliding mode observer and extended Kalman filter for sensorless vector control of induction motor drives”. In: (2009), pp. 2466–2473.

# Appendices

# Appendix A

## Technical background

Equation 3.6 can be rewritten in stationary reference frame as:

$$\psi_{s\alpha} = \int (V_{s\alpha} - R_s i_{s\alpha} - U_{comp,\alpha})dt \tag{1}$$

$$\psi_{s\beta} = \int (V_{s\beta} - R_s i_{s\beta} - U_{comp,\beta})dt \tag{2}$$

Equation 3.15 can also be rewritten in stationary reference frame as:

$$U_{comp,\alpha} = \left[K_p + \frac{K_p}{T_I}\int dt\right]\left(\psi^v{}_{s,\alpha} - \psi^i{}_{s,\alpha}\right) \tag{3}$$

$$U_{comp,\beta} = \left[K_p + \frac{K_p}{T_I}\int dt\right]\left(\psi^v{}_{s,\beta} - \psi^i{}_{s,\beta}\right) \tag{4}$$

Once the stator flux linkages in equation 1 and 2 are calculated, the rotor flux linkages based on the voltage model are computed as:

$$\hat{\psi}_{r\alpha} = \frac{1}{k_r}\hat{\psi}_{s\alpha} - \frac{\sigma L_s}{k_r} i_{s\alpha} \tag{5}$$

$$\hat{\psi}_{r\beta} = \frac{1}{k_r}\hat{\psi}_{s\beta} - \frac{\sigma L_s}{k_r} i_{s\beta} \tag{6}$$

$$\theta_e = \tan^{-1}\left(\frac{\psi_{r\beta}}{\psi_{r\alpha}}\right) \tag{7}$$

## Discrete time analysis

From equation 3.33, it is possible to extract the rotor flux linkage dynamics in synchronously rotating reference frame as:

$$\frac{d\psi_{rd}}{dt} = \frac{L_m}{\tau_r} i_{sd} - \frac{1}{\tau_r}\psi_{rd} \tag{8}$$

As in [3], applying backward Euler-based approximation on equation 8:

$$\frac{\psi_{rd}(k) - \psi_{rd}(k-1)}{T} = \frac{L_m}{\tau_r} i_{sd}(k) - \frac{1}{\tau_r}\psi_{rd}(k) \tag{9}$$

where T is the sampling time. Rearranging equation 9

$$\psi_{rd}(k) = \left(\frac{\tau_r}{\tau_r + T}\right)\psi_{rd}(k-1) + \left(\frac{L_m T}{\tau_r + T}\right) i_{sd}(k) \tag{10}$$

$$\frac{d\psi_{s\alpha}}{dt} = e_{s\alpha} \tag{11}$$

where $e_{s\alpha}$ back emf
Equation 3.6 can be discretized as follows:

$$\frac{d\psi_{s\alpha}}{dt} = \frac{\psi_{s\alpha}(k) - \psi_{s\alpha}(k-1)}{T} = e_{s\alpha}(k) \tag{12}$$

Assuming that the dynamics of the mechanical system are much slower than the dynamics of the electric variables, we may assume that the motor back emf does not change during an observer sampling period[1].

$$e_{s\alpha}(k) = e_{s\alpha}(k-1) \tag{13}$$

So it is possible to write equation 12 as:

$$\frac{d\psi_{s\alpha}}{dt} = \frac{\psi_{s\alpha}(k) - \psi_{s\alpha}(k-1)}{T} = \frac{1}{2}(e_{s\alpha}(k) + e_{s\alpha}(k-1)) \tag{14}$$

Rearranging equation 14

$$\psi_{s\alpha}(k) = \psi_{s\alpha}(k-1) + \frac{T}{2}\left(e_{s\alpha}(k) + e_{s\alpha}(k-1)\right) \tag{15}$$

Following the same method:

$$\psi_{s\beta}(k) = \psi_{s\beta}(k-1) + \frac{T}{2}\left(e_{s\beta}(k) + e_{s\beta}(k-1)\right) \tag{16}$$

The back emf can be determined from equation 1 and 2: differentiating both equations with respect to time:

$$\frac{d\psi_{s\alpha}}{dt} = e_{s\alpha}(k) = V_{s\alpha}(k) - R_s i_{s\alpha}(k) - U_{comp,\alpha}(k) \tag{17}$$

$$\frac{d\psi_{s\beta}}{dt} = e_{s\beta}(k) = V_{s\beta}(k) - R_s i_{s\beta}(k) - U_{comp,\beta}(k) \tag{18}$$

PI control laws are discretized as follows:

$$\frac{dU_{comp,\alpha}}{dt} = \frac{d\left(K_p\left({\psi^v}_{s,\alpha} - {\psi^i}_{s,\alpha}\right)\right)}{dt} + \frac{d\left(\frac{K_p}{T_I}\int\left({\psi^v}_{s,\alpha} - {\psi^i}_{s,\alpha}\right)dt\right)}{dt} \tag{19}$$

$$\frac{dU_{comp,\beta}}{dt} = \frac{d\left(K_p\left({\psi^v}_{s,\beta} - {\psi^i}_{s,\beta}\right)\right)}{dt} + \frac{d\left(\frac{K_p}{T_I}\int\left({\psi^v}_{s,\beta} - {\psi^i}_{s,\beta}\right)dt\right)}{dt} \tag{20}$$

$$\frac{dU_{comp,\alpha}}{dt} = K_p\left(\frac{d\psi^v{}_{s,\alpha}}{dt} - \frac{d\psi^i{}_{s,\alpha}}{dt}\right) + \frac{K_p}{T_I}\left(\psi^v{}_{s,\alpha} - \psi^i{}_{s,\alpha}\right) \tag{21}$$

$$\frac{dU_{comp,\beta}}{dt} = K_p\left(\frac{d\psi^v{}_{s,\beta}}{dt} - \frac{d\psi^i{}_{s,\beta}}{dt}\right) + \frac{K_p}{T_I}\left(\psi^v{}_{s,\beta} - \psi^i{}_{s,\beta}\right) \tag{22}$$

$$\frac{d\psi^v{}_{s,\alpha}}{dt} = \frac{d\psi^i{}_{s,\alpha}}{dt} \tag{23}$$

$$\frac{dU_{comp,\alpha}}{dt} = \frac{K_p}{T_I}\left(\psi^v{}_{s,\alpha} - \psi^i{}_{s,\alpha}\right) \tag{24}$$

$$\frac{d\psi^v{}_{s,\beta}}{dt} = \frac{d\psi^i{}_{s,\beta}}{dt} \tag{25}$$

$$\frac{dU_{comp,\beta}}{dt} = \frac{K_p}{T_I}\left(\psi^v{}_{s,\beta} - \psi^i{}_{s,\beta}\right) \tag{26}$$

Applying backward Euler approximation to equations 24 and 26:

$$\frac{U_{comp,\alpha}(k) - U_{comp,\alpha}(k-1)}{T} = \frac{K_p}{T_I}\left(\psi^v{}_{s,\alpha}(k) - \psi^i{}_{s,\alpha}(k)\right) \tag{27}$$

$$\frac{U_{comp,\beta}(k) - U_{comp,\beta}(k-1)}{T} = \frac{K_p}{T_I}\left(\psi^v{}_{s,\beta}(k) - \psi^i{}_{s,\beta}(k)\right) \tag{28}$$

After some rearrangement:

$$U_{comp,\alpha}(k) = U_{comp,\alpha}(k-1) + \frac{TK_p}{T_I}\left(\psi^v{}_{s,\alpha}(k) - \psi^i{}_{s,\alpha}(k)\right) \tag{29}$$

$$U_{comp,\beta}(k) = U_{comp,\beta}(k-1) + \frac{TK_p}{T_I}\left(\psi^v{}_{s,\beta}(k) - \psi^i{}_{s,\beta}(k)\right) \tag{30}$$

### Speed estimator

From equation 3.33, it is possible to determine rotor flux linkages $\psi_{r\alpha}$ and $\psi_{r\beta}$:
Then it is possible to determine the magnitude and the rotor flux angle from the current model.

$$\psi_r = \sqrt{{\psi_{r\alpha}}^2 + {\psi_{r\beta}}^2} \tag{31}$$

$$\theta_e = \tan^{-1}\left(\frac{\psi_{r\beta}}{\psi_{r\alpha}}\right) \tag{32}$$

Differentiating equation 32 with respect to time:

$$\sec^2\theta_e \frac{d\theta_e}{dt} = \frac{\psi_{r\alpha}\frac{d\psi_{r\beta}}{dt} - \psi_{r\beta}\frac{d\psi_{r\alpha}}{dt}}{\psi^2{}_{r\alpha}} \tag{33}$$

$$\sec^2\theta_e = \left(\frac{\psi_r}{\psi_{r\alpha}}\right)^2 \tag{34}$$

Substituting equation 3.33 into 33:

$$\omega_r = \frac{1}{{\psi_r}^2}\left[\left(\psi_{r\alpha}\dot{\psi}_{r\beta} - \psi_{r\beta}\dot{\psi}_{r\alpha}\right) - \frac{L_m}{\tau_r}\left(\psi_{r\alpha} i_{s\beta} - \psi_{r\beta} i_{s\alpha}\right)\right] \tag{35}$$

Discretizing equation 35 gives:

$$\omega_r(k) = \frac{1}{|\psi_r|^2}\left[\left(\psi_{r\alpha}(k-1)\psi_{r\beta}(k) - \psi_{r\beta}(k-1)\psi_{r\alpha}(k)\right) - \frac{L_m}{\tau_r}\left(\psi_{r\alpha}(k) i_{s\beta}(k) - \psi_{r\beta}(k) i_{s\alpha}(k)\right)\right] \tag{36}$$